Preparation of model cobalt catalysts for Fischer-Tropsch synthesis using ultrasound preparation techniques

Thesis submitted in partial fulfilment for the requirements of the M.Sc. degree in Chemical Engineering at the University of Cape Town

by

Willem Johannes Erasmus

M.Sc (Physics) UOFS

Supervisor : Prof. E van Steen

Cape Town

2006

Acknowledgements

I would like to sincerely thank the following people for their help and assistance during this study:

Prof. E van Steen for his excellent guidance

Dr. TH Dlamini for guidance and many interesting discussions

Sasol Technology Research and Development for their financial assistance and the opportunity to take part in this Taught Masters Program

Mrs. B Breedt and Mrs E du Plessis for their help with the XRD analyses

Dr. E Mokoena for her assistance with the hydrogen chemisorption analyses

Mr. D Morgan for suggesting the cannulation method

My wife Belinda for her dedication and support

Declaration

I know the meaning of plagiarism and declare that all the work in the document, save for that which is properly acknowledged, is my own.

Abstract

In order to study the oxidation behaviour of small cobalt crystallites during Fischer-Tropsch synthesis, it is necessary to prepare model catalysts with cobalt crystallites of which the size distributions can be adjusted. Here ultrasonication was used to decompose a tricarbonyl nitrosyl cobalt precursor in n-decane to prepare small cobalt crystallites. The aim of this study was to vary the cobalt crystallite size distribution by adjusting the preparation conditions. Transmission Electron Microscopy (TEM) was used to measure the crystallites and to obtain the crystallite size distributions.

Ultrasonication of the plain precursor/solvent solution created small cobalt crystallites that were unstable and prone to sintering. More stable materials were prepared by either incorporating silica powder as a support material, or by adding oleic acid as a stabilizing agent to form colloidal particles.

The cobalt crystallite size distribution did not change with time during 20 hours of ultrasonication. The concentration of the precursor was varied by adding between 0.625g and 5g of the precursor to 100ml n-decane. The temperature of the solution was varied between 20°C and 60°C, and the ultrasound amplitude was varied between 20% and 60% of the maximum setting on the equipment. In all cases no effect on the cobalt crystallite size distribution was observed.

The size of the crystallites formed by this process was much smaller than one would anticipate from the contents within a bubble prior to the cavitation event. There were significant differences in the crystallite size distributions between the unsupported, the silica supported and the oleic acid-stabilized materials. It was postulated that a bubble implosion event does not form a single crystallite from the cobalt material contained within the bubble, but that many crystallites are formed. The presence of silica powder or oleic acid provides extra nucleation sites and therefore influences the amount and size of the crystallites formed.

Table of Contents

1 Introduction

1.1 General introduction

The synthesis of fuels and chemicals from non-petroleum-based feedstock such as coal, natural gas or biomass is a viable alternative to oil-based chemistry. Although oil is still the largest contributor to the world total primary energy demand, the Fischer-Tropsch process has applications in cases where special circumstances make the conversion of other carbon sources into liquid fuels a viable technology.

A carbon source of interest nowadays is natural gas. Worldwide there are huge reserves of economically accessible natural gas reserves[1, 2]. According to Dry[1] the ratios of crude oil to methane to coal reserves presently known are 1:1.5:25 (measured as oil equivalent). Thus, production of syngas from methane or coal will become more important as the reserves of crude oil are depleted or, as is currently the case, the price of crude oil rises.

Areas which currently have a high potential for implementation of a natural gas-based Fischer-Tropsch process are the European North Sea, Alaska and countries around the Arabian Gulf[3]. In these and other regions such as Western Africa environmental legislation may also increase the demand for the high quality products of the Fischer-Tropsch process, or even for the process itself, in order to dispose of methane associated with oil wells and residual heavy oils.

1.1.1 Historical development of Fischer-Tropsch synthesis

Several reviews were written that describe the historical development of the Fischer-Tropsch process[3, 4, 5]. Here a short summary is given of the most important developments.

The origin of the Fischer-Tropsch process is often attributed to the work of Senderens and Sabatier in 1902. They discovered that nickel catalyzes the conversion of synthesis gas to methane at high temperature. However, in the 1920's Franz Fischer and Hans Tropsch synthesised higher hydrocarbons from CO and H_2 using various metals such as iron, cobalt and nickel, thereby laying the foundation for the Fischer-Tropsch process as we know it today.

The early studies showed that nickel and cobalt were more promising catalysts since iron produced mainly oxygenates. However, these studies were performed at atmospheric pressure due to the fact that BASF had patented processes in 1913 for making hydrocarbons and oxygenates by the hydrogenation of CO on oxide catalysts at higher pressures. It was only in 1937 that Fischer and Pichler discovered that the product spectrum on iron as well as the lifetime of the iron catalyst improved significantly by operating at higher pressures.

The early 1930's saw the development of Ni-ThO_2-kieselguhr and Co-ThO_2-kieselguhr catalysts. Initial studies concentrated on the nickel catalyst since it was more easily obtainable than cobalt. However, in pilot plant and larger reactors it was found that nickel tended to make too much methane and had a short lifetime. As a result further developments concentrated on the development of a process based on cobalt-based catalysts.

In 1935 the first commercial operation of the Fischer-Tropsch process was started in Germany, using a cobalt catalyst. The German Fischer-Tropsch reactors operated throughout the 2^{nd} world war and produced about 20% of the gasoline used in Germany at the time. During this period there was a drive to replace the cobalt catalyst with an iron catalyst, but this never materialized. The operation of the Fischer-Tropsch plants in Germany was discontinued after the end of the war.

For a short time after the war there was significant interest in the Fischer-Tropsch process in the USA, England and West Germany. In the USA the interest was driven by a fear of an impending shortage of petroleum. But in the 1950's petroleum became abundant and inexpensive due to the discoveries of huge oil deposits in the Middle East, which led to the termination of most of the coal-to-oil research and development programs.

In the early 1970's the USA started to import oil to supplement its own production. Research in the Fischer-Tropsch process experienced a short revival after the oil crises in the Middle East which resulted in a fourfold increase in the price of petroleum. In 1982 the world-wide recession decreased the demand for petroleum, leading to a very low oil price and little interest in coal-to-oil enterprises.

In 1955 the Sasol Fischer-Tropsch plant for the conversion of coal to petroleum products was built and commissioned. This plant originated as a result of the world wide fears of increasing crude oil prices, but also due to the fact that large reserves of coal could be mined at a low price[6]. Prompted by the oil crisis of the mid 1970's and the sharply rising price of crude oil, Sasol extended its operations in 1980 and 1982 by the building of the Sasol II and Sasol III plants.

In 1992 the Mossgas plant was built in South Africa to exploit the off-shore natural gas reserves. This facility made use of Sasol's circulating fluidised bed reactors and produced mainly gasoline and diesel[6]. At first this plant operated at a loss due to the low crude oil price of about US$ 15 per barrel[1]. It became operationally profitable in 1999 when the oil price rose above US$ 40 per barrel.

In 1993 Shell also erected a Fischer-Tropsch plant in Malaysia that produces high quality diesel fuel and waxes from natural gas. In this fixed bed operation a cobalt catalyst is used rather than the iron catalyst used in the Mossgas operations.

1.1.2 Economical aspects

In Europe methane is sold as fuel in competition with gas oil. For this reason the value of methane in any part of the world tends to be linked to sales in Europe. The price that the household consumer is willing to pay for gas makes it too expensive for a large industrial natural gas conversion plant[2]. However, in areas that are far away from Europe gas can be obtained at a price that is more suitable for industrial conversion processes.

One such area is Qatar, which has very little oil reserves, but vast natural gas reserves. Qatar does not have a great demand for gas and is thus able to sell it cheaply. Another interesting case where gas can be obtained relatively cheaply, is Nigeria. This country has strict legislation that prohibits the flaring of methane associated with crude oil in new oil refineries/wells. Here the natural gas has a negative value since it has to be either pumped back into the earth (adding to costs), or converted into products.

Long distance piping of natural gas is expensive and may become politically risky if the pipeline has to pass through other countries. Liquefying the gas will require specially designed tankers for transport and becomes uneconomical beyond a certain distance. It is

thus more sensible to convert the gas to liquid products and transport it using normal tankers[7].

The Fischer-Tropsch process offers a viable route for converting natural gas into more valuable liquid products. According to Gradassi[8] the Fischer-Tropsch process has "broken through the profitability barrier" as a result of technological improvements in syngas generation, reactor design, catalysts and overall process scalability. The economical viability of a new Fischer-Tropsch plant was assessed by assuming a base-case scenario (with parameters such as a plant capacity of 50 000 bpd, liquid product value = 143% of crude oil price, a natural gas price of $0.50 per MSCF, a crude oil price of $18.00 per barrel, etc.). The results indicated that the manufacturing cost of the product adds up to about $14.00 per barrel, which can be considered as the break-even point for the investment. An Internal Rate of Return (IRR) of 15%, which is considered attractive for many investors, can be realised if the product is sold for $26.00 per barrel. This price is achievable at a crude oil price of $18.00 per barrel. Even at a crude oil price of $14.00 per barrel an IRR of 10% is feasible. Jager[9] also states that, at crude oil prices in the $16.00 – $18.00 per barrel range, the product prices are expected to lie in the $22.00 – 25.00 range and a pre-tax return on the investment of 12 – 15% can be realised.

Gradassi[8] also illustrated the sensitivity of the economics to factors such as the price of gas, the plant capital cost, the crude oil price and the liquid product value. The price of gas was found to have the largest influence, which highlights the fact that an attractive gas price must be secured over the lifetime of the manufacturing plant.

The most expensive process in a Fischer-Tropsch plant is the production of synthesis gas. In a coal-based process this accounts for about 60 - 70% of the capital and running costs[1, 6]. In the process about 50% of carbon is converted to CO_2 due to the fact that the water-gas-shift reaction is required to compensate for the low hydrogen content in coal. The capital cost of a methane conversion plant is about 30% lower than that of a coal gassification plant. In addition, only about 20% of the carbon is converted to CO_2, which makes this process more efficient.

The Fischer-Tropsch process is only one of several gas-to-liquid technologies, competing with other processes such as methanol synthesis and dimethyl-ether production[8].

However, the Fischer-Tropsch process has some advantages which makes it an attractive option. One advantage is that the product blends well with crude oil and can be pumped with it[9]. Conversion to methanol, on the other hand, would require a separate transport system.

The high quality products that are produced by the Fischer-Tropsch process may also fetch a premium in the market[9]. For instance, the diesel produced by this process has a high cetane number (around 74 compared to a cetane number of 40 for conventional US diesel), very low sulphur levels and a very low aromatic content[7]. (The low sulphur content in the Fischer-Tropsch product is due to the necessity to remove all sulphur compounds upstream from the Fischer-Tropsch reactors due to the sensitivity of the Fischer-Tropsch catalyst to sulphur poisoning.) Furthermore, the emission levels for hydrocarbons, CO, NO_x and particulate matter of the Fischer-Tropsch diesel is significantly lower than for conventional diesel. This product is thus an ideal blending stock for upgrading certain crude oil derived diesel fractions[9, 10].

1.1.3 New operations in Nigeria and Qatar

Natural gas can be obtained at reasonably economical prices in Qatar and Nigeria, which makes these countries ideal for running the Fischer-Tropch process to convert the gas to more valuable liquid products. Sasol is currently in the process of erecting Fischer-Tropsch synthesis plants in these two countries. In the latter case Sasol has entered into a mutually beneficial partnership with ChevronTexaco, who plan to open new oil wells and find an economical way of disposing of the associated gas.

1.1.3.1 Choice of process

The Fischer-Tropsch reaction produces a wide variety of products with different carbon chain lengths and structures. By selecting suitable operating conditions the product distribution can be directed towards a certain kind of product so that the yield of this product is significantly increased. There is generally a distinction between High Temperature (300 – 350 °C) and Low Temperature (200 – 250 °C) Fischer-Tropsch synthesis.

The highly linear and low aromatic content of the products of the Low Temperature Fischer-Tropsch reaction are ideal for the production of diesel with a high cetane number. The maximum yield of diesel that can be obtained from the product spectrum is about 25%[6], but by shifting the selectivity of the process to higher carbon numbers to form waxes and applying selective mild hydrocracking, the total diesel yield is increased to about 73%.

High Temperature Fischer-Tropsch synthesis is the best option if the desired product is gasoline, since the product yield is about 40 mass% straight run gasoline in the C_5-C_{11} range. Furthermore, propene and butene, which makes up about 20% of the product stream, can be dimerised to gasoline products. The straight run gasoline, however, has a low octane number due to its high linearity and low aromatic content[1]. Several downstream processes are required to improve the octane number, thus making the overall process complex[7]. This process is currently in place at the Sasol plants in Secunda. Low Temperature Fischer-Tropsch synthesis is more suitable for the conversion of natural gas in remote gas fields to liquids[9] since it requires less downstream processes. It should however be noted that on a larger scale the high temperature Fischer-Tropsch process also becomes more viable since the advantages obtained from the chemicals outweigh the disadvantages of the greater work-up costs and complexities.

1.1.3.2 Choice of reactor

The original reactors used by Sasol for the production of wax, were the Tubular Fixed Bed (so-called ARGE) reactors[6, 11]. These reactors are still in operation. Extruded iron catalyst particles are packed into tubes about 12 m long and 5 cm in inner diameter. Each reactor contains about 2050 of these tubes, which are surrounded by cooling water to remove the heat of reaction. The synthesis gas passes downwards through the tubes and the wax product trickles down and is recovered at the bottom (see Figure 1-1). The Fischer-Tropsch reactors being used by Shell in Malaysia are of a similar design, except that the tubes are thinner in order to compensate for the higher temperature sensitivity of cobalt-based catalysts[1].

An alternative to the TFB reactor is the slurry reactor which was originally studied by Fischer. The first unit was commissioned in 1953 by Kölbel[6]. This reactor consists of a

vessel that contains the catalyst particles suspended in the product. Figure 1-1 shows a schematic comparison of the two different reactor types. Synthesis gas is bubbled from the bottom through this suspension and the agitating effect ensures that the particles are kept in suspension. The reactor is typically more isothermal that fixed bed reactors. The synthesis gas diffuses from the bubbles through the liquid phase to the catalyst where it reacts to form the products. The heat generated is removed via cooling coils that are in contact with the suspension liquid inside the reactor[9].

Initially the further development of this reactor for Fischer-Tropsch industrial application was held up due to the lack of a suitable method to separate the catalyst particles from the wax product. In 1990 Sasol developed a workable solution to this problem and in 1993 a 22 m high and 5 m wide slurry reactor was successfully commissioned.

The slurry reactor has several advantages over the Tubular Fixed Bed reactor which also resulted in it being the reactor of choice for the Fischer-Tropsch facilities planned for Qatar and Nigeria[10, 11]. One of the biggest advantages is that it is much simpler than the Tubular Fixed Bed reactor and therefore much cheaper to construct. The reactor can also be scaled much more easily so that full advantage can be taken of the economy of scale.

Another major advantage is the more isothermal environment inside the reactor due to the agitating effect of the gas bubbles on the catalyst suspension. This eliminates the axial and radial temperature gradients that are experienced in the Tubular Fixed Bed reactor. The temperature can thus be better controlled and a higher average temperature can be maintained, leading to higher production. This makes it possible to use a catalyst with a higher activity.

The slurry reactor also has a much larger yield per unit mass of catalyst than the TFB reactor. This is attributed to the higher average temperature at which it can be operated, but also due to the fact that smaller particles are used in this reactor, thereby minimising diffusion limitations.

Other advantages that contribute significantly to the economic viability of the process are the lower pressure drop over the reactor (which saves on recompression costs) and the

ability to add or remove catalyst on-line without the need for costly and labour intensive catalyst replacement.

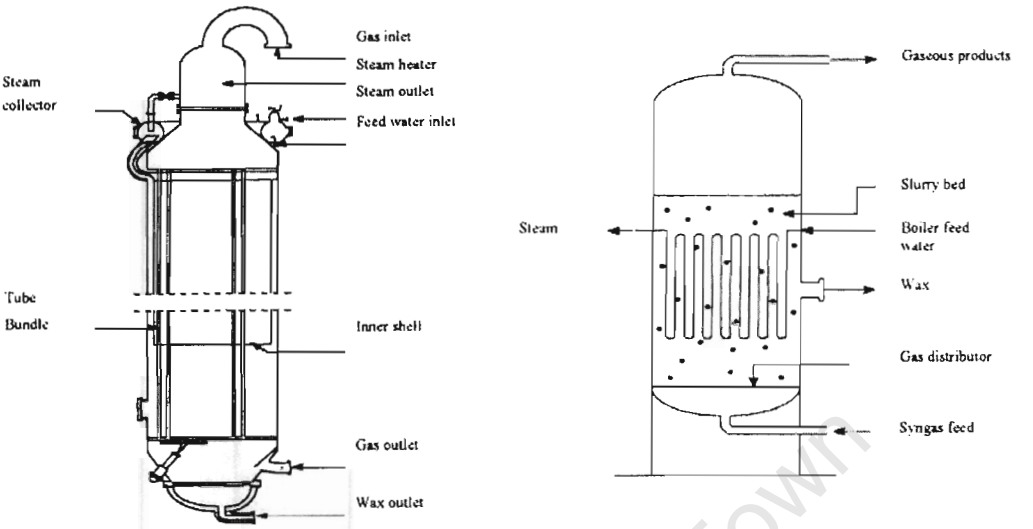

Figure 1-1 Schematics of the Tubular Fixed Bed reactor and the Slurry reactor (Espinoza et al.[10])

1.1.3.3 Choice of catalyst

Although all the group VIII transition metals[12] and some other metals such as Mo[13] have the ability to catalyse the Fischer-Tropsch reaction, only iron and cobalt are used commercially. The catalytic activity of most of the metals is too low for economic application, or mostly oxygenated products are produced due to the fact that CO does not adsorb dissociatively on these compounds. Nickel makes too much methane at practical operating conditions and is generally used as a methanation catalyst. Ruthenium seems to be a very good catalyst for Fischer-Tropsch synthesis, but unfortunately it is far too expensive and there is not enough available for industrial application. In 2002 the relative price of iron, nickel, cobalt and ruthenium was approx. 1 : 250 : 1000 : 50 000[1].

Iron catalysts are used for both high temperature and low temperature synthesis, whereas cobalt is only used for low temperature synthesis due to its higher methane selectivity at higher temperatures[1]. Sasol currently performs low temperature Fischer-Tropsch synthesis using fixed bed (ARGE) reactors with a precipitated iron catalyst. The main reason for using the iron catalyst is due to its low price.

The new Fischer-Tropsch plants that are constructed for Nigeria and Qatar will make use of a cobalt catalyst instead of iron. Cobalt has some advantages over iron, such as a higher activity, longer lifetime and its suitability for the methane feedstock.

The lifetime of the iron catalyst in a tubular fixed bed reactor is typically a few weeks. One of the deactivation mechanisms is the deposition of carbon on the catalyst surface via the Boudouard reaction[5]. The deposited carbon builds up in the pores of the catalyst and forces the catalyst particles to break. According to Adesina[13], cobalt does not have the same tendency to produce elemental carbon compared to iron.

The cobalt catalyst is also more suitable for the methane feed that is to be used in the new Gas-to-Liquid plants. The Fischer-Tropsch process requires a molar ratio of hydrogen to carbon monoxide of around 2:1. Coal has a relatively low hydrogen content and the water-gas-shift reaction is required to adjust the H_2:CO ratio to the required levels. This makes iron, which is an active catalyst for this reaction, suitable for applications where coal is the feedstock. Reforming of natural gas, however, yields a H_2:CO ratio that is close to 2, which means that the water-gas-shift reaction is not required. Since cobalt has very low water-gas-shift activity, it is thus more suitable for use with natural gas feedstock. As a direct result, the emission of CO_2 is greatly reduced during the manufacture of the synthesis gas from methane, resulting in higher carbon efficiency.

Van Berge and Everson[14] compared the activities of an iron and cobalt catalyst at different space velocities at 20 bar pressure with a H_2:CO feed ratio of 2:1. They concluded that, at these conditions and low space velocities, cobalt has a higher activity than iron. This was ascribed to the fact that the performance of the cobalt catalyst is not inhibited as much as iron by the water partial pressure in the reactor, which increases with conversion.

Water is known to affect the Fischer-Tropsch reaction rate on iron-based catalysts. The kinetic equation determined by Dry et al.[6] shows that an increase in the water partial pressure inhibits the rate of reaction. For cobalt-based catalysts, however, the kinetic equation determined by Yates and Satterfield[15] contains no inhibition term for the water partial pressure.

$$r = \frac{mp_{H2}p_{CO}}{p_{CO} + ap_{H2O}}$$

Iron-based catalyst

$$r = \frac{kp_{H2}p_{CO}}{(1 + bp_{CO})^2}$$

Cobalt-based catalyst

Thus, iron-based catalysts can only be used at relatively low conversions. At high conversion levels the rate of reaction rate will be inhibited by water. As a consequence synthesis gas needs to be recycled since it is rather costly. For the iron Fischer-Tropsch process higher overall conversions can only be achieved by removing the water from the exit gas stream[9]. This adds to the capital cost and requires additional recompression. Since cobalt-based catalysts are not strongly affected by the water partial pressure, a higher per pass conversion can be achieved under Fischer-Tropsch synthesis conditions.

1.2 Catalyst deactivation by water

Water formed by the Fischer-Tropsch process has a tendency to oxidise the iron catalyst particles to an inactive oxide state[11]. This is usually observed in the increase of the water-gas-shift activity, which is believed to take place on magnetite. The oxidation of cobalt by the product water is also considered to be a deactivation mechanism for the cobalt catalyst[1,16].

1.2.1 Thermodynamic considerations

According to Anderson[4] the equilibrium constant (P_{H2O}/P_{H2}) for the reaction $CoO + H_2 \leftrightarrow Co + H_2O$, will be between 150 and 57.5 in the 127-427 °C temperature range. This implies that the reaction is favoured towards the right and that oxidation of cobalt metal to CoO by water is unlikely to occur. This was confirmed by van Berge et al.[17] when they compared the P_{H2} / P_{H2O} ratios found under typical Fischer-Tropsch conditions (0.86 - 2.00) to the above thermodynamic data. They concluded that the water partial pressure under these conditions is not enough to push the above reaction to the left (see Figure 1-2).

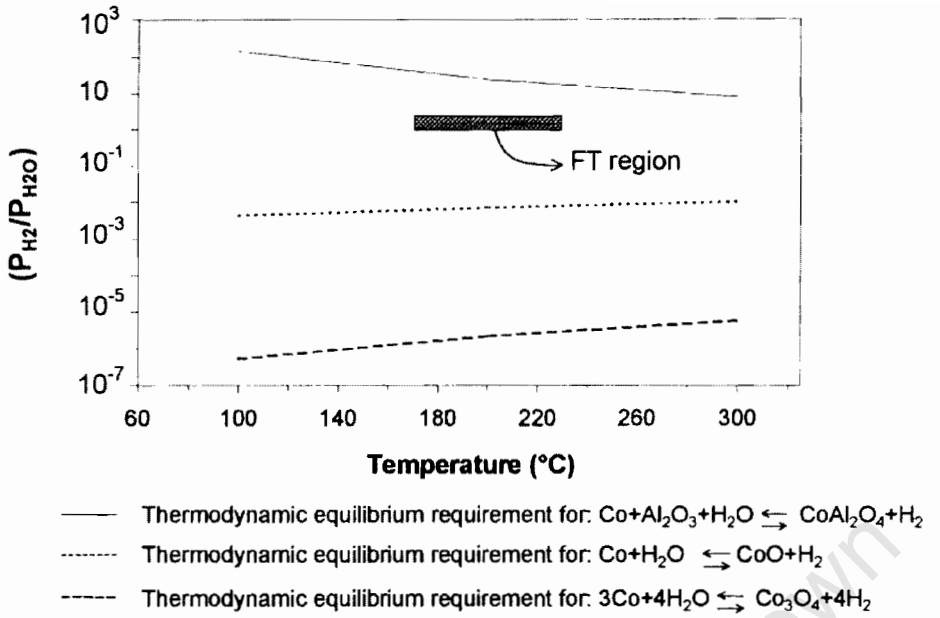

Figure 1-2 Thermodynamic calculations on the oxidation of metallic cobalt to CoO (van Berge et al.[17])

The oxidation of bulk cobalt is clearly not feasible under Fischer-Tropsch synthesis conditions. However, other researchers have reported oxidation of small crystallites by the water produced during Fischer-Tropsch synthesis[1, 16]. Van Steen et al.[18] performed thermodynamic calculations that showed that, under typical Fischer-Tropsch synthesis conditions (P_{H2O}/P_{H2} < 1.5, 220 °C), metallic cobalt crystallites smaller than 4.4 nm will be unstable and will consequently oxidize to Co(II)O. This is because the surface energies of metal oxides are generally lower than those of metals. The ratio of surface atoms to bulk atoms becomes larger as crystallites become smaller. Thus, the surface energy contribution will dominate in nanosized materials.

It must be noted that van Berge et al.[17] found that, for the reaction $Co + Al_2O_3 + H_2O \leftrightarrow CoAl_2O_4 + H_2$, the oxidation of cobalt is thermodynamically spontaneous under typical Fischer-Tropsch conditions. They concluded that this reaction is kinetically restricted since significant amounts of cobalt aluminate do not form during the calcination pre-treatment at temperatures lower than 500 °C, and since relatively severe hydrothermal treatment of the catalyst is required to form the cobalt aluminate spinel.

1.2.2 The surface of the alumina supported cobalt catalyst

Arnoldy et al.[19] utilised a combination of Temperature Programmed Reduction (TPR) and X-ray Diffraction (XRD) in order to elucidate the different phases that can occur on the surface of an alumina supported cobalt catalyst. TPR spectra of samples calcined at different temperatures showed that four types of surface species can occur. The first, reduced at around 327 °C, are Co_3O_4 crystallites similar to bulk Co_3O_4. The second type, which is reduced at around 477 °C, belongs to surface Co^{3+} ions or mixed Co^{3+}-Al^{3+} oxide crystallites. The third type is attributed to surface Co^{2+} species, while the fourth type consists of several species including subsurface Co^{2+} ions in a diluted, ill-defined Co^{2+}-Al^{3+} spinel, and $CoAl_2O_4$ crystallites. The relative amounts of these four phases were influenced by the calcination pre-treatment temperature. A similar description of the catalyst surface was later provided by Schanke et al.[20] in order to explain their observed catalyst deactivation behaviour.

Tung et al.[21] performed a similar study on alumina supported catalysts with various cobalt loadings that were calcined at a fixed temperature of 500 °C. They found that, at low loading, reduction only occurred after 577 °C, whereas more reduction peaks at lower temperatures were observed at higher loading. EPR measurements at various peak temperatures led them to assign the TPR peak at 347 °C to Co^{3+} species and the peak at 517 °C to Co^{2+} species.

Various researchers used techniques such as XPS[22], Raman[23] and XANES[24] in order to probe the structure of the various phases. Although these phases are frequently referred to as cobalt-aluminate-like phases, there is consensus that the phases reducing at these temperatures are different from stoichiometric $CoAl_2O_4$.

1.2.3 Effect of water on activity of alumina supported catalysts

Van Berge et al.[17] performed experiments where they compared the activity of two catalysts in two separate synthesis tests. After an initial stabilisation period during which both catalysts showed similar deactivation and activity profiles, water was co-fed to one of the reactions. A fast decline in activity was seen, after which the activity profile stabilised and no further deactivation was observed. When the extra water supply was removed, the activity remained unchanged, indicating that the severe deactivation treatment of the water had a permanent effect.

Hilmen et al.[22] performed a similar investigation on the activity decrease of both a Re promoted and unpromoted cobalt catalyst. When high water partial pressures were introduced during the reaction, rapid deactivation of the promoted catalyst was observed. After removal of the water from the feed, the activity of the catalyst remained at the lower level, but no further deactivation was apparent. The unpromoted catalyst showed similar behaviour, but the relative decrease in activity was less than for the promoted catalyst.

Li et al.[25] investigated the oxidation of a Pt promoted Co/Al_2O_3 catalyst under Fischer-Tropsch synthesis by either lowering the feed rate in order to increase conversion, or by adding varying amounts of water to the feed. Lower feed rates resulted in higher catalyst deactivation rates. If the feed rate is lowered by a small amount, the CO conversion declined rapidly to a certain level where it reached a new stable conversion level. However, when the feed rate was lowered too much, the CO conversion declined continuously. They noticed a slight decrease in the CO conversion upon the addition of a small amount of water to the feed. The activity was recovered when the water to the feed was terminated and the catalyst was not permanently affected by the brief operating period with water in the feed. However, increasing the water feed too much resulted in a severe and irreversible deactivation of the catalyst.

In other studies the effect of water was investigated by subjecting the catalysts to feeds with different H_2O/H_2 ratios. Hilmen et al.[26] found that the extent of re-oxidation depended on the H_2O partial pressure and the H_2O/H_2 ratio. This was confirmed by van Berge et al.[17] who found that, for low hydrogen partial pressures, the cobalt oxidises completely, whereas oxidation takes place to a certain level at higher hydrogen partial pressures. Also, the oxidised metal could be fully recovered by re-reduction when oxidation took place at lower temperatures (150 °C). At higher temperatures (200-300 °C), however, only a fraction of the oxidised metal could be recovered.

TPR analyses of the 'oxidised' catalyst samples showed the presence of species that reduce in the temperature range between 377 °C, where Co_3O_4 reduces, and 927 °C where $CoAl_2O_4$ is reduced[20]. The peaks in this region are frequently referred to as well dispersed Co^{2+} and Co^{3+} species that are similar to cobalt aluminate. Zhang et al.[27] found

that 92% of the cobalt was reduced during a standard reduction treatment (350 °C for 12 hours), while the reduction degree was reduced to about 45% by the addition of only 3% water vapour to the hydrogen feed. By adding water vapour to the feed during a TPR experiment they could see that the first reduction peak at around 250 °C (ascribed to the reduction of Co_3O_4) remained essentially at the same temperature with the same H_2 consumption with increasing water content to the feed. The second peak was found to shift to higher reduction temperatures as the water content was increased.

Promotion of the cobalt catalyst with elements such as Pt, Re and Ru has the effect of increasing the degree of reduction of the catalyst[22, 23, 26]. Schanke et al.[22, 26, 28] found that Re or Pt promoted cobalt catalysts had a higher H_2 uptake during H_2-chemisorption analyses than their unpromoted counterparts. This usually indicates a better dispersion of the active metal, but can also indicate that small crystallites that were not reduced on the unpromoted catalyst, were indeed reduced in the promoted catalyst. The cobalt dispersion calculated from XRD line broadening or hydrogen chemisorption experiments was similar for both the unpromoted and the promoted catalysts[22, 28].

TPR analyses of unreduced catalysts showed that the high temperature peaks in the 427 – 727 °C regions were lowered by as much as 100 °C for the promoted catalyst[20]. This indicates that the promoter has the effect of aiding the reduction process rather than increasing the dispersion. Li et al.[25] suggested that reduction of the cobalt particles occurs by nucleation and growth and that Pt may increase the rate of nucleation of sites by hydrogen spill-over.

Schanke et al.[20] proposed that well dispersed cobalt species that are not reduced in unpromoted catalysts during standard reduction procedures, are reduced in promoted catalysts. This results in the higher activity of these catalysts, but also in the enhanced rate of oxidation due to the instability of these well dispersed cobalt species. This faster deactivation rate may be due to the higher water partial pressures produced by the higher catalyst activity[24].

In conclusion, there is substantial evidence to suggest that cobalt can oxidize under Fischer-Tropsch conditions, leading to deactivation of the cobalt catalyst. It is suspected that the nano-sized crystallites are especially prone to oxidation. This needs to be verified

by synthesizing nano-sized crystallites in model catalysts and investigating their deactivation behaviour.

1.3 Ultrasound

1.3.1 General introduction

In chemistry the interaction between energy and matter is often important for obtaining the desired chemical product at a suitable rate. Ultrasound irradiation is an alternative method of adding energy to a system with characteristics that is somewhat different from the traditional energy sources such as heat or light.

The first observations of the chemical effects of ultrasound were reported by Richards and Loomis[29] in 1927. They reasoned that ultrasound irradiation of a chemical solution causes a series of standing waves that exist of nodes, which are relatively 'untroubled' regions, and loops where varying tension in the liquid occurs. An increase in energy density (higher temperature) occurs during the compression cycle so that chemical reactions should proceed at a higher rate in these regions. A slowdown in the reaction rate should occur in the expanded regions where the temperatures should be cooler. For some chemical reactions the increased reaction rate in the compressed regions should not be offset by the decline in the rate in the expanded region, thus leading to an increased overall reaction rate. An increase in reaction rate was indeed observed in several reactions.

A closely associated phenomenon of ultrasound is the weak emission of light by certain solutions under ultrasound irradiation. Sonoluminescence of water was observed for the first time in 1935 by Frenzel and Schultes[30]. They postulated that the formation of H_2O_2 in water under ultrasound irradiation could be due to a charge separation effect which causes O_2 to be mechanically ionised. When they looked for an accompanying discharge, they found that water emits light when it is exposed to ultrasound irradiation. According to Sehgal et al.[31] the sonoluminescence observed is due to the formation of an excited water molecule by the ultrasound process, which can then either undergo a radiative relaxation (emitting a photon at 270 – 290 nm) or dissociation into OH and H radicals (emitting a photon at 310 nm).

In earlier times the 'electrical discharge' theory was the accepted mechanism for sonoluminescence. According to Henglein[32] the discharge theory is no longer regarded as being correct. Sehgal et al.[31] showed that the electrical participation in the production of excited species will be negligibly small compared to that arising from thermal origins.

Suslick and Kemper[33] also argued against the electrical theory of sonoluminescence by investigating the sonoluminescence from $Cr(CO)_6$ in silicone oil containing various dissolved gases. The gases were CO, N_2, CF_4, C_2F_6 and the noble gases. The intensity of sonoluminescence is influenced by the value of γ (=Cp/Cv); low γ-values are usually associated with poly-atomic gases and will decrease the intensity of Cr* emission. It was found that even 1% mixtures of the perfluorocarbon gases substantially suppressed the sonoluminescence. This is in direct conflict with electrical discharge theories since CF_4 is known to be an efficient gas for plasma chemistry and will support an electrical discharge. It is now generally accepted that the water molecules are thermally excited via the acoustic cavitation process.

1.3.2 The mechanism of ultrasound effects

Acoustic cavitation can be described as the formation, growth and implosive collapse of bubbles in a liquid caused by sound passing through the liquid [34]. During the collapse of the bubbles regions of very high temperature and pressure are formed due to the adiabatic compression of the bubble implosion. These regions give rise to the thermal excitation of molecules responsible for sonoluminescence.

A sound field causes compression and expansion cycles within regions in the liquid. The formation of cavities occur when the expansion cycle is intense enough to pull the liquid apart. However, according to Suslick et al.[35, 36] cavitation is a nucleated process since the tensile strength of a pure liquid is so large that the formation of a cavity from the negative pressure of an acoustic cycle is unlikely (for water more than 1000 atm of negative pressure will be required). Instead, bubbles are formed at weak points in the liquid such as gas filled crevices in small solid particles, or already existing bubbles within the liquid. This is supported by the fact that Frenzel and Schultes observed no luminescence in outgassed water[30].

Two types of bubbles are formed in the irradiated solution, viz. stable and transient cavities[32]. Transient cavities generally exist for less than one cycle of the sound field during which they expand to many times their original size before collapsing violently. Stable cavities exist for longer periods that can last for many cycles.

The expansion and compression cycles produced by the ultrasound cause a stable bubble to oscillate about a certain equilibrium radius. The stable cavity can grow in size due to a process of rectified diffusion: During the expansion cycle gas diffuses into the bubble due to the lower partial pressure inside the bubble. The reverse happens during the compression cycle as gas diffuses out of the bubble. However, the rate of diffusion into or out of the bubble is dependant on the surface area of the bubble. Since the wall of the bubble is larger during the expansion cycle that during the compression cycle, more gas will diffuse into the bubble than will diffuse out of the bubble during the compression cycle, thus causing the oscillating bubble to slowly grow in size.

The growing bubble will eventually reach a critical size where it will absorb energy from the ultrasound most efficiently. This size corresponds to the natural vibration frequency of the bubble and depends on the frequency of the ultrasound wave. At this stage the bubble can grow rapidly within a single cycle. Once the bubble has grown past this critical size, it can no longer efficiently absorb energy from the sound field and can no longer sustain itself. Forces such as the static pressure and the surface tension start to dominate and the bubble becomes very unstable. With the next compression cycle the surrounding liquid rushes in and the bubble implodes.

1.3.3 The conditions inside the collapsing bubble

The pressures and temperatures due to the adiabatic compression caused by the cavitating bubbles are believed to be very large. The maximum temperature and pressure of a gas-filled bubble were calculated to be approximately 10 000 °C and 12 000 bar[37]. Henglein[32] reported the calculations of Fitzgerald who estimated the maximum temperature to be 7423 °C.

The measurement of the conditions inside a collapsing bubble using normal methods is not possible due to the transient nature of the cavitation event[36]. However, the effective temperature can be determined by measuring the rate of chemical reaction from these

bubbles and comparing it to the rate of a certain reaction of which the temperature dependency of the rate has already been determined. The use of this method ('comparative-rate chemical thermometry' using the sonochemical ligand substitution rates of volatile metal carbonyls as probe reaction) showed the existence of two regions of sonochemical activity[38]. The first corresponds to the gas phase inside the cavitating bubble and reaches an effective temperature of approx. 4927 ± 650 °C. The second corresponds to a thin liquid layer surrounding the collapsing cavity and reaches a temperature of approx. 1627 °C.

The pressure that is reached during the implosion of a bubble is harder to determine experimentally than the temperature. Suslick[36] estimated the peak pressure to reach about 500 atm, assuming adiabatic conditions. The cooling rate after the implosion was estimated to be more than a billion °C per second.

The implosion event also lasts for a very short time. Barber et al.[39] measured the emitted sonoluminescence pulses of light from a glycerine in water solution during ultrasonication using a photomultiplier tube (PMT). The output from the PMT had a rise time of 2.2 ns before reaching the maximum. The same rise time was observed when a laser pulse of 34 ps was incident on the PMT, thus indicating that the emission time of the sonoluminescence pulse was less than the limitations of the PMT. Using a PMT with a rise time of 240 ps, the same result was again obtained. On the latter findings they based a conservative upper limit of 100 ps for the pulse duration.

The peculiar and violent nature of ultrasound irradiation is also apparent in its interaction with suspended solids. When a solid surface immersed in a liquid is subjected to ultrasound, localised erosion of the surface takes place and characteristic microscopic pitting is observed. This is caused by a combination of two effects, although their relative importance has not yet been established. Firstly, the asymmetry of the region near the solid-liquid interface induces a deformation in the collapsing cavity. This results in the emission of a fast-moving stream of liquid through the cavity towards the surface with velocities greater than 100 m/s [40]. The high-speed liquid jet from a collapsing bubble created by a laser beam has been filmed by Lauterborn and Vogel[41] using a rotating mirror camera at 75 000 frames per second. The second mechanism of surface damage

arises from the shock waves from the collapsing cavity in the liquid. The erosion of the surface by the microjets and shock waves explains the process of ultrasonic cleaning.

In contrast to extended solid surfaces, small particles are too small to influence the cavitating bubble. At 20 kHz, for example, Neppiras[37] calculated that a collapsing bubble will have a diameter of approx. 150 μm. Solid particles smaller than this size cannot cause the formation of microjets. Instead, shock waves generated by the cavitational collapse can cause small particles to collide into one another. The speed at which these particles collide depends upon the size of the particles. Doktycz et al.[42] observed that inter-particle collisions and melting result in the formation of a neck of metal that joins two particles. By investigating particles of different metals with different melting points, they determined that these necking structures, and therefore the temperature at the point of collision between the particles, form between 2600 and 3400 °C for two particles 10 μm in diameter. The impact velocities of these particles were estimated to be between 100 and 500 m/s.

1.3.4 Preparation of materials using ultrasound

The very high localised temperatures and pressures as well as the high cooling rates of ultrasound irradiation provide researchers with a novel method to synthesise catalysts and other industrially important materials. This method often offers advantages over conventional preparation methods.

The most common method of preparation is to ultrasonicate a solution containing a volatile organometallic compound. The volatile compound diffuses into the stable bubbles formed by the ultrasound. When the bubbles collapse, the high temperatures and extreme conditions cause the compound to decompose and to form small particles.

Suslick and co-workers[43] have synthesised a variety of nano-structured inorganic materials by irradiating solutions of volatile organometallic compounds with high intensity ultrasound. In this way they produced high-surface-area solids that are agglomerates of nanometer clusters. These clusters can subsequently be trapped as colloids (using polymeric ligands such as polyvinylpyrrolidone) or supported materials (using oxide supports such as silica or alumina).

A silica-supported amorphous nano-structured iron catalyst was prepared by ultrasonic irradiation of iron pentacarbonyl in the presence of silica gel[43]. TEM images showed that the resulting iron particles ranged in size from 3-8 nm and were well dispersed on the silica surface. The Fischer-Tropsch activity of this catalyst (iron loading = 10.94 wt%, dispersion = 1.85%) was compared to that of a conventionally prepared silica-supported iron (iron loading = 9.91 wt%, dispersion = 1.86%) prepared by incipient wetness impregnation. This comparison was done at temperatures ranging from 200-330 °C with a feed of H_2/CO = 3.48. The pressure at which these tests were performed was not indicated. They found that the sonochemically prepared catalyst was an order of magnitude more active than the conventionally prepared catalyst. This was attributed to the amorphous nature of the iron and the highly defected surfaces formed during ultrasonication.

Fe-Co alloys were prepared by using various mixtures of $Fe(CO)_5$ and $Co(CO)_3(NO)$ as precursors[43]. This resulted in small alloy clusters that were homogeneous on a nanometer scale. After heat treatment under H_2 gas flow for 2 hours at 400 °C these clusters crystallised into clusters between 10 and 20 nm. It was found that the alloy was a good dehydrogenation catalyst, whereas the pure metals showed very little dehydrogenation activity.

Nano-structured Mo carbide can also be synthesised using sonochemical methods by ultrasound irradiation of Mo hexacarbonyl in hexadecane followed by heat treatment at 450 °C for 12 hours under He. This yielded small Mo_2C crystallites that were active for the dehydrogenation of cyclohexane reaction, while inactive for the hydrogenolysis reaction.

Shafi et al.[44] used a similar preparation method and precursors to produce nano-sized amorphous Fe-Ni-Co alloys (<10 nm). In the usual preparation method a glass former (B, P, Si or Al) is added to lower the melting point so that the alloy can be quenched rapidly enough to be kept in the amorphous phase. The presence of the glass former, however, has a marked influence on the magnetic properties of the alloy. The ultrasound preparation method takes advantage of the rapid cooling rate experienced in the 'hot spot' of the imploding bubble and eliminates the need for the glass former.

Wang et al.[45] prepared copper monosulfide and nickel monosulfide nanoparticles. An aqueous solution containing the metal acetate ($Cu(CH_3COO)_2$ or $Ni(CH_3COO)_2$) and thioacetamide in the presence of triethanolamine as a complexing agent was ultrasonicated with 20 kHz ultrasound under air. TEM images showed that the CuS crystallites were about 13 nm and the NiS crystallites were about 17 nm.

Lead sulfide nanocrystals were prepared using a similar method[46]. Here an aqueous solution of lead acetate, sulphur toluene and sodium lauryl sulfate (added as surfactant) was ultrasonicated to produce crystallites with an average size of 11 nm. A particle size distribution is shown with the majority of crystallites ranging between 8 and 14 nm.

Ultrasound irradiation can also be used in other ways to synthesise nano-sized materials. Henglein and co-workers[47] prepared colloidal solutions of MoS_2 and WSe_2 for semiconductor applications. The usual method of preparation (precipitation of metal ions by corresponding hydrogen chalcogenide) often resulted in the metal being reduced to an undesired lower valence state. In the ultrasonication method a small amount of the powdered semiconductor material was added to water and exposed to ultrasound under an atmosphere of 80% Ar and 20% H_2. The ultrasound caused very small fragments to split off from the particles rather than causing a gradual crushing of the larger particles. After filtration to remove most of the large particles, the ultrasonicated solution contained a distribution of large particles (50 to several 1000 nm) as well as very small particles (<10 nm).

Ultrasound can also enhance crystallisation[48]. The expansion phase of the cavitational bubble causes a localised cooling where an increase in the degree of supersaturation is experienced. This leads to the formation of nuclei which are distributed throughout the medium after the bubble has collapsed. Consequently, catalyst particle sizes are reduced compared to the conventionally prepared catalysts. During the preparation of zeolites he observed that ultrasound application led to substantial reduction in nucleation time and overall completion times. It also resulted in smaller particles. A similar effect was observed by Amara et al.[49], who found that the crystallisation of potash alum from an aqueous solution of potassium aluminium sulfate hydrate was affected by the implementation of ultrasound. They noted that the ultrasound irradiation resulted in

smaller crystals with narrower crystallite size distribution. Interestingly, the shape of the crystals was decahedra instead of the octahedra that was found without the application of ultrasound.

Bianchi et al.[50] used various methods to prepare silica-supported cobalt-based catalysts for Fischer-Tropsch synthesis, which included incipient wetness impregnation of the support with an aqueous cobalt nitrate solution. Ultrasound irradiation was implemented in two of these methods by (1) adding the impregnated catalyst to pure hydrazine at 80 °C and exposing to ultrasound for 15 min, and (2) adding the cobalt nitrate solution to the support under ultrasonication at room temperature for 1 h. All the catalysts contained 5 wt% cobalt and were tested for 4 days at 275 °C and 500 kPa with a feed consisting of $H_2/CO = 2$. The former catalyst performed the worst amongst all the catalysts tested, whereas the latter had the best performance.

1.3.5 Factors that influence the effect of ultrasound

There are several factors that influence the effects of ultrasound on the rate of reaction or the intensity of sonoluminescence. Some of these factors were also shown to have an influence on the characteristics of synthesised materials.

Frequency

One of the first parameters that one would suspect to play a role in the interaction of ultrasound with liquids, is the frequency. Pétrier et al.[51] investigated the rate of phenol and carbon tetrachloride degradation in water by the OH radicals formed during ultrasound exposure. Solutions were exposed to four different ultrasound frequencies ranging between 20 and 800 kHz (30 W acoustic power, 20 °C). The maximum rate of phenol degradation was found to occur at 200 kHz. For carbon tetrachloride degradation, however, the rate of degradation was faster at 800 kHz that at the other tested frequencies, and the degradation rate depended weakly on the frequency.

Keck et al.[52] also observed a frequency dependence of the yield of H_2O_2 in pure water. However, in their case they found that the maximum yield occurred between 400 – 600 kHz. It is difficult to explain why their results differ from those of Pétrier et al[51]. One possible reason, mentioned by Pétrier et al., is that "the formation and behaviour of the bubble is closely linked to the sound pressure field which depends of the reactor (design)

and of the ultrasonic source (frequency, surface emitting area, intensity)". For instance, the study by Pétrier et al. was performed on 300 ml of solution and the energy output was adjusted to deliver a power of 30 W to the solution. In the study by Keck et al. 500 ml of solution was ultrasonicated with a power of 100 W. No information regarding the vessels used in these studies were provided. It is interesting to note, though, that the study by Keck et al. focussed on the influence of small particles on the rate of degradation of several organic contaminants. By adding 10 g/liter of quartz particles (3-10 μm) the maximum rate of H_2O_2 formation occurred at a frequency of around 200 kHz. Furthermore, this rate is about 50% higher than for pure water alone.

Hoffman et al.[53] noticed that ultrasonic frequencies in the range 300 – 1000 kHz did not increase the rate of C-alkylation of benzyl cyanide by 2-bromopropane. However, the reaction rate was significantly enhanced by 25 kHz ultrasound. This was attributed to an increased implosion time, size of cavitation bubbles and mechanical mixing effects.

Precursor vapour pressure

The organometallic precursor should be highly volatile since the primary sonochemical reaction site is in the vapour phase inside the cavitating bubble. Suslick and co-workers[38] varied the vapour pressure of iron pentacarbonyl by increasing the solution temperature and showed that the sonochemical rate coefficient depends linearly on the vapour pressure of the metal carbonyl. This effect can have a marked influence in the preparation, especially if binary or ternary compounds are prepared. Shafi et al.[54] experienced this problem during the sonochemical preparation of Co-Ni alloys using ultrasound irradiation of $Co(NO)(CO)_3$ and $Ni(CO)_4$. The latter compound had a vapour pressure far higher than the former, so that an excess of the former had to be introduced in order to obtain the correct stoichiometry of the alloy.

Precursor concentration

The particle size of the sonication products can be controlled by varying the concentration of the precursor in the irradiated solution[55]. Takatani et al.[56] prepared Au/Pd particles by ultrasonicating nobel metal complexes of these metals in water. The average sizes of the particles varied between 7.0 and 11.7 nm, depending on the concentrations of the metal complexes.

Solvent type and vapour pressure

The bubbles formed during ultrasound exposure do not only contain gas from the precursor, but also vapours from the solvent. Solvent molecules usually have a low γ-value, which decreases the maximum temperature reached during cavitation. Furthermore, the solvent vapour is compressible and strips energy away from the adiabatic heating process. Solvent molecules can also undergo their own sonochemical reactions, thus removing energy from the bubble and decreasing the temperature reached during cavitation[57]. More volatile solvents will therefore reduce the effective temperature during bubble collapse.

Suslick and co-workers[57] found during ultrasound irradiation of $Fe(CO)_5$ that, at high solvent vapour pressure, the cavitational temperature was lowered so that mostly ligand substitution reactions and cluster formation took place. At conditions favouring maximum cavitational heating, (low vapour pressures and with some Ar dissolved gas), loss of multiple ligands occurred, resulting in the formation of metal particles.

Dissolved gas

In addition to the precursor and the solvent, any dissolved gases in the liquid can have a significant effect on the ultrasound effects. The sonochemical reactivity is influenced by the value of γ (=Cp/Cv). Monatomic gases have the highest values for γ (to around 1.67) and thus cause the highest temperatures during cavitation, whereas poly-atomic gases have a γ-value approaching 1 and result in less heating during adiabatic collapse.

In the study by Henglein[47] discussed above very little fragmentation was observed when the powders were ultrasonicated under an atmosphere of pure hydrogen. Henglein also reported the enhanced sonoluminescence intensities observed in water with dissolved Ar or Xe.

The thermal conductivity of the gas is also important[57]. As an example, He and Ar have the same γ-value (1.67) and should thus reach the same final temperature during cavitation. It has been observed, however, that He decreases the rates of most sonochemical and sonoluminescence processes. This effect was attributed to the higher

thermal conductivity of He (0.149 $Wm^{-1}K^{-1}$) as compared to Ar (0.0172 $Wm^{-1}K^{-1}$), which lowers the peak temperature reached during cavitation.

Sehgal et al.[31] observed that the intensity of sonoluminescence emission in the presence of inert gases increases with atomic number (i.e., He < Ne < Ar < Kr). The sonoluminescence spectra of Ne, Ar and Kr saturated solutions had a very similar intensity distribution, which suggested that these gases do not participate chemically in the sonoluminescence process. Also, the noble gases did not appear in any end products and no emissions from the excited states of these gases were observed. Gases like N_2, O_2 or air, however, resulted in much lower sonoluminescence intensities than the noble gases. These gases may also have participated in the radical transformation reactions and were seen in the end products. Interestingly, they also observed that the sonoluminescence intensities from O_2- and N_2-saturated solutions were weaker than those from air-saturated solutions.

Temperature of solution

Didenko et al.[58] studied the effect of the temperature of Ar saturated water on the sonoluminescence intensity (10-75 °C) and found that the sonoluminescence intensity diminished with the increase of temperature. This was attributed to the decrease in the gas concentration in the water at higher temperatures, thus increasing the water vapour pressure in the bubble and thereby decreasing the temperature of the bubble when it implodes. Similar trends were observed for ultrasound frequencies of 22 kHz, 337 kHz and 1.1 MHz.

Ultrasound amplitude

Li-yun et al.[59] produced hydroxyapatite powder by ultrasonication of $Ca(NO_3)_2$, $NH_2H_2PO_4$ and NH_2CONH_2 in water at various conditions. They found that the hydroxyapatite particles increased in size as the Ca^{2+} concentration is increased and decreased in size as the temperature is increased. Furthermore, at power settings lower than 300 W a mixture of hydroxyapatite and other phases formed, while at higher settings only hydroxyapatite was obtained. The particle sizes of this hydroxyapatite phase decreased linearly as the ultrasonic power was increased.

Ultrasonication time

Few studies report on the influence of ultrasound time. Li et al. [60] report that the size of their InP particles increased with ultrasonication time. For ultrasonication times between 4 and 6 hours the final particles (determined using XRD analyses) increased from 9 to 27 nm. For ultrasonication times longer than 6 hours there was no change in particle size. According to their explanation, this increase in particle size was as a result of interparticle collisions causing localized heating. They also postulated that the nanoparticles formed contained a large number of dangling bonds and defect sites, which were reduced by growth of the crystallites during the ultrasound process until they reached a more stable surface state.

Zhang et al.[61] prepared silver nanorods and nanofibers by combining reverce micelle and ultrasound techniques. They found that the length of the nanofibers could be increased by increasing the ultrasonication time. Wang et al.[62], on the other hand, found that the ultrasonication time had no influence on the size of their CeO_2 nanoparticles that were prepared by ultrasonication of $(NH_4)_2Ce(NO_3)_6$ in poly ethylene glycol. Similarly, Wang et al.[46] found that the sizes of their nanocrystallites were not influenced by the ultrasonication time.

1.4 Aim of this investigation

Studies on the alumina-supported cobalt catalyst have shown the presence of so-called well-dispersed cobalt phases that have a stronger interaction with the support than large Co_3O_4 crystallites. These species are difficult to reduce during a standard reduction treatment, but adding a promoter such as Re or Pt to the catalyst results in the lowering of the reduction temperatures of these phases and their subsequent reduction.

However, these species are also easily oxidised again by water that is formed during the Fischer-Tropsch reaction, as was shown by experiments where water was added to the reactor feed. This deactivation depends on the ratio of the water and hydrogen partial pressures and can be reversible or permanent, depending on the reaction conditions.

It has also been reported in the literature that the addition of a small amount of water to the catalyst during reduction has a significant negative effect on the reduction degree[23]. Although this is easily preventable in the laboratory, it is more difficult on an industrial

scale where the water formed during reduction has to diffuse through the catalyst bed before being removed from the reactor system. This illustrates the importance of understanding the interaction of water with the catalyst in order to minimise these conditions as much as possible.

It has been suggested in the literature that there is a certain threshold crystallite size where oxidation of the crystallites becomes favourable. For example, Li et al.[25] observed differences in the oxidation behaviour of silica and alumina supported catalysts, but mentioned the possibility that the different cobalt crystallite sizes (5.7 nm for alumina supported and 13.2 nm for silica supported) may explain this different behaviour rather than the nature of the support. Iglesia[16] postulated that this threshold crystallite size is around 5-6 nm. Van Berge et al.[63] however, believe that this threshold is around 10.3 nm, while the thermodynamic calculations of van Steen et al.[18] suggest that oxidation of metallic cobalt crystallites smaller than 4.4 nm will occur under typical Fischer-Tropsch synthesis conditions.

As this threshold crystallite size will aid in the understanding of the dynamics of the catalyst and in improving and optimising the catalyst performance, stability and lifetime, it is very important to try and identify this threshold crystallite size. In order to study the oxidation of small metallic cobalt crystallites, model supported catalysts with narrow and adjustable size distributions need to be prepared for testing under synthesis conditions.

In this study it was attempted to prepare cobalt catalyst materials with crystallite sizes that can be easily varied. The literature studies discussed above showed that a variety of materials can and have been prepared. The fact that these materials generally have different crystallite sizes suggest that it may be possible to vary the crystallite size distribution of the prepared nanostructures. For the purpose of this study the aim was to show that this can be accomplished by varying the preparation conditions. No study was found in literature where the preparation conditions were systematically varied with the specific purpose to manipulate the crystallite sizes of the final product.

The hypothesis for this investigation was as follows :
Using an ultrasound preparation method, the cobalt crystallite size distribution can be manipulated in the nanometer range by adjusting the preparation conditions.

The materials for this study were prepared by ultrasound irradiation of a solution consisting of n-decane, an organometallic cobalt compound (tricarbonyl nitrosyl cobalt) and a dissolved gas (argon). The effects of the following parameters on the cobalt crystallite size were systematically studied :

- Ultrasonication time
- Precursor concentration
- Ultrasound intensity
- Ambient temperature

The crystallite sizes of the prepared materials were evaluated using X-ray diffraction (XRD), Transmission Electron Microscopy (TEM) and hydrogen chemisorption.

2 Experimental

2.1 Equipment used

2.1.1 Ultrasound synthesis equipment

In this study a Vibracell model GEX600 ultrasonic instrument from Sonics and Materials Inc. was used to provide ultrasound irradiation (see Figure 2-1). This unit can provide high intensity ultrasound with a power output of up to 600 Watt. The instrument and the ultrasound frequency are similar to those used by several other researchers for preparing materials with this method[43, 44]. The high tensile strength of liquids makes it difficult for bubbles to form in the liquid so that a high intensity ultrasound probe is the most effective instrument for performing lab scale sonochemistry[40]. Li et al.[60] showed that they could produce InP nanocrystals using ultrasound equipment similar to those used in this study, but they could not produce these nanocrystals at low intensities (such as those produced by a commercial ultrasonic cleaner).

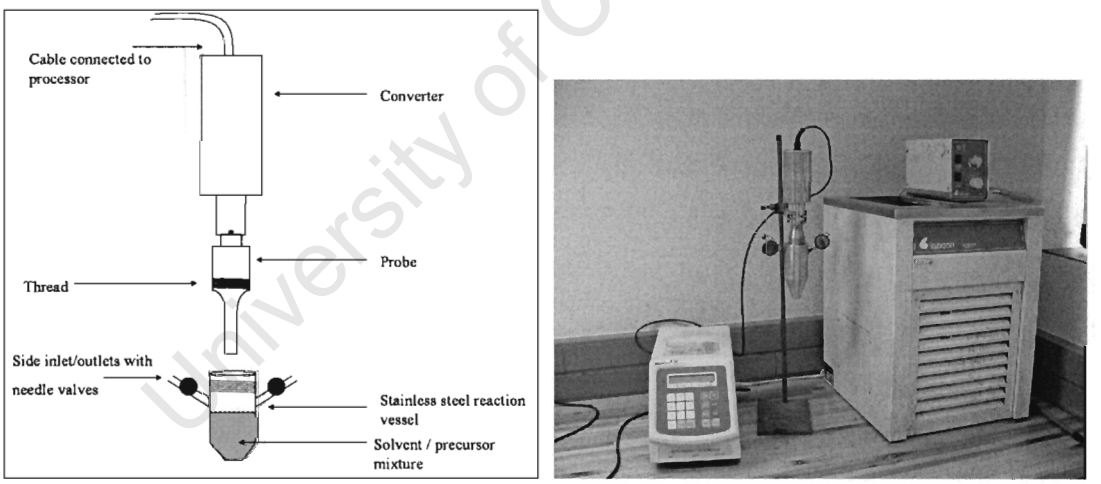

Figure 2-1 A scetch of the ultrasound converter, probe and reaction vessel (left) and a photograph of the ultrasound equipment (right). In the photograph the ultrasound processor is on the left, the ultrasound converter and probe with the reaction vessel screwed on is supported by the retort stand, and the Labcon cooling bath is on the right.

The instrument consists of the following[64] :

- An Ultrasonic processor, which converts the 50 Hz electricity from the main supply to high frequency (20 kHz) electrical energy. The frequency of the ultrasound was fixed at 20 kHz and could not be changed.
- The converter, which contains a piezoelectric transducer that converts the electrical energy to mechanical vibrations.
- The probe, which is in contact with the liquid and intensifies the vibrations. The probe is specifically designed to resonate at the frequency provided by the converter.

The probe is made from a titanium alloy and has a 38 mm body diameter stepped to 13 mm radiating diameter. For preparations in water a probe with a removable tip that can easily and cheaply be replaced, is usually employed. This is because the violent cavitation events at the probe tip gradually cause damage to the surface of the tip, which eventually renders the probe ineffective. However, liquids with low surface tension (solvents in general) penetrate the interface between the probe and the replaceable tip and carry small particles into the threaded section[64]. As a result the tip is isolated from the probe so that the probe no longer resonates at 20 kHz and the power supply will fail. Since the experiments in this study were conducted in a low-surface tension medium, a solid probe was acquired.

In these preparations the liquid was exposed to ultrasound inside a stainless steel vessel that screws tightly onto the ultrasonic probe. The cobalt precursor is quite volatile at ambient conditions, which makes it necessary to confine the precursor/solvent mixture in a closed vessel. The steel vessel has a volume of 135 ml and has two side inlets that are closed off by needle valves. A pressure test of the closed vessel/probe assembly was performed by pressurising the vessel with air at 2 bar and monitoring the pressure for 30 minutes using a pressure indicator. No pressure loss was observed during this period.

The temperature inside the reaction vessel was regulated by immersing the vessel in a Labcon low temperature water bath.

The ultrasound probe was tuned before each preparation. By tuning the probe, the frequency provided by the processor is matched to that of the converter/probe assembly,

thereby optimising its performance and ensuring that the maximum amount of energy is transferred.

2.1.2 Other equipment

In most preparations n-decane and the cobalt precursor were transferred to the reaction vessel in a 280 litre polyethylene atmosbag, which was purchased from Sigma-Aldrich. Since the cobalt precursor decomposes readily in atmosphere and forms poisonous fumes the bag was flushed with argon in order to create an inert atmosphere. This bag was also used to unload the products formed from the reaction vessel since the cobalt product formed during the ultrasound process was in the metallic state and exposure to atmosphere would lead to fast oxidation and subsequent sintering. The argon gas entered the bag via a silicon tube installed in the side of the atmosbag. As a safety measure the atmosbag was situated inside a fumehood.

2.2 Preparation of materials

2.2.1 Materials used

The precursor, tricarbonyl nitrosyl cobalt, was purchased from Alfa Aesar. This dark red liquid was packaged in sealed vials containing 5g of the precursor. Contradictory information regarding the physical properties and, in particular, the vapour pressure and the boiling point of this compound were found in the literature (see Table 2-1 and Figure 2-2). The vapour pressure data indicated by Ivanova et al.[65] and Liley et al.[66] concur. The difficulty in the determination of the actual boiling point of cobalt tricarbonyl nitrosyl is likely to be associated with the decomposition of this compound.

Table 2-1 Physical properties of tricarbonyl nitrosyl cobalt

Chemical formula	$Co(NO)(CO)_3$
T_{boil} at 760 mmHg	48.6 °C[a]/80 °C[66]
$T_{decomposition}$	55 °C[a]
Density, ρ	2.09 g/cm^3 at 20 °C[a]
ΔH^{vap}	35.7 kJ/mol[b]

[a] Boiling point/decomposition temperature indicated by Alfa-Aesar and Handbook of Physics and Chemistry; density indicated by Alfa-Aesar

[b] Estimated using the Clausius-Clapeyron equation on the data given by Ivanova et al.[65] and Liley et al.[66]

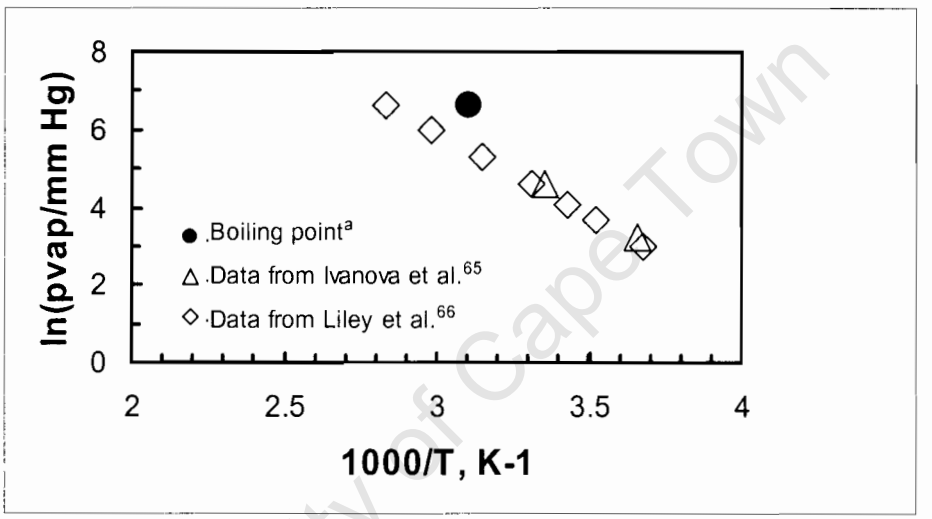

Figure 2-2 Vapour pressure of Co(CO)3(NO) as a function of temperature.

[a] Boiling point indicated by Alfa-Aesar and Handbook of Physics and Chemistry

n-Decane was used as solvent due to its high boiling point. Anhydrous n-decane was obtained from Sigma-Aldrich. Table 2-2. lists some of the physical properties of this compound that are of interest to this study.

Table 2-2 Physical properties of n-decane

Chemical formula	$C_{10}H_{22}$
T_{boil}	174 °C
Density, ρ	0.73 g/cm^3 at 20 °C
Surface tension, γ	23.37 mN/m at 25 °C
Viscosity, μ	0.838 mPas at 25 °C
Thermal conductivity, k	0.132 W/m K at 25 °C
Vapour pressure, p^{vap}	1.8 mmHg at 25 °C

Argon (Afrox) was used to flush the atmosbag and to enhance the effects of ultrasound in the solvent. The purity was 99.999% (N5.0), while the oxygen content was less than 2 vppm and moisture less than 1 vppm.

The silica support material used for one set of preparations was a silica powder supplied by Engelhard, De Meern B.V. It was a high purity material with low levels of contaminants. The BET surface area was 80 m^2/g, the pore volume was 1.0 ml/g and the average pore diameter was 50 nm. The particles were spherical and ranged from 75 – 500 μm in size.

Other chemicals used in this study were :

- Oleic acid with a purity of 99.9%, obtained from Saarchem (Pty) Ltd. This compound was chosen as a stabilizer for the cobalt crystallites due to the fact that it has worked well in previous preparations of iron crystallites.
- n-Pentane (oil free) with a purity of 99.9%, obtained from Associated Chemical Enterprises (Pty) Ltd.
- Ethanol absolute (99.8%), obtained from Sigma-Aldrich.

2.2.2 Filling the reaction vessel

Most of the preparations made use of the atmosbag to ensure that the n-decane and precursor did not come into contact with air. The ultrasound probe/converter, reaction vessel and chemical containers were placed into the atmosbag. The bag was flushed at least three times with argon by alternate filling and evacuation (using a rotary pump) cycles.

100 ml of n-decane was transferred to the reaction vessel. The n-decane was saturated with argon gas by bubbling the gas for a period of at least 30 minutes through the liquid. The rate of argon flow could not be accurately controlled and was thus not measured, but it caused significant agitation of the liquid and was estimated to be at least 200 ml(STP)/min.

Where required, the silica support or oleic acid stabilizer was added to the solvent. The precursor was then quickly added and the ultrasound probe screwed onto the vessel. The vessel was then immersed in the water bath and left for a period of 30 minutes in order to allow the temperature to adjust to the temperature of the water.

In the preparation of the silica-supported materials, the atmosbag was not utilised since it had developed tears and leaks that could not be repaired. For these samples the saturation process was carried out in air, but the mouth of the reaction vessel was covered with tin foil in order to restrict the access of air to the n-decane. The cobalt precursor was added in air to the solvent and the vessel quickly closed. The contact of the precursor with air was limited and only a small amount of air was trapped inside the vessel so that this process had a negligible effect on the preparation.

2.2.3 Utrasonication

An overview of the materials prepared in this study is presented in Table 2-3. The conditions of preparation were kept constant with only one parameter being varied at a time. The temperature of the solution was normally kept at 10 °C, while the amplitude setting was set at 40%.

Table 2-3 Overview of materials prepared

No.	Precursor (g)	SiO_2 (g)	Oleic acid (ml)	Time (min)	Temp. (°C)	Amplitude (%)	Passivation
t0	5	-	-	30	10	40	At. bag
t1	0.625	-	-	30	10	40	At. bag
t2	0.625	-	-	300	10	40	At. bag
t3	0.625	-	-	600	10	40	At. bag
t4	0.625	-	-	1200	10	40	At. bag
C1	5	3	-	1800	10	40	canul
C2	2.5	1.5	-	1800	10	40	canul
C3	1.25	1.5	-	1800	10	40	canul
C4	0.625	1.5	-	1800	10	40	canul
T1	5	-	5	120	10	40	At. bag
T2	1.25	-	5	120	35	40	At. bag
T3	1.25	-	5	120	60	40	At. bag
A1	1.25	-	5	120	10	20	At. bag
A2	1.25	-	5	120	10	60	At. bag

Influence of ultrasound exposure time

This first experiment served two purposes. Firstly, it gave an indication of the rate at which the product was formed, so that a time could be identified at which a sufficient amount of product was formed for further characterization. Secondly, effects such as the high temperature caused by interparticle collisions or the decrease in precursor concentration as more product material is formed, can have an influence on the nature of the resulting material. It was thus important to investigate whether the ultrasound exposure time had an influence on the size of the cobalt crystallites.

Samples t1 to t4 were prepared by adding 0.625 g ($1/8^{th}$ vial) of precursor to 100 ml n-decane and ultrasonicating the solution at normal conditions (T = 10 °C, amplitude = 40%). After specific times (30 minutes, 5 hours, 10 hours and 20 hours respectively) the

ultrasonication process was interrupted and the vessel was returned to the atmosbag where TEM samples were obtained from the suspension in the vessel.

Influence of precursor concentration

The tricarbonyl nitrosyl cobalt was supplied in sealed glass vials containing 5g of the precursor. Due to the volatility of this compound, smaller amounts could not be extracted from these vials. Smaller concentrations were obtained by preparing and diluting a parent solution of the contents of one vial in 100 ml argon-saturated n-decane. The resulting solution was transferred to a 100 ml volumetric flask, which was stored in a fridge at 4 °C.

In order to halve the precursor concentration, 50 ml of the parent solution was extracted and mixed in the reaction vessel with a further 50 ml of argon-saturated n-decane. Similarly, the concentrations were reduced by a factor of 4 (or 8) by mixing 25 ml (or 12.5 ml) of the parent solution with 75 ml (or 87.5 ml) of saturated n-decane.

In these experiments silica was added as a support in order to stabilise the cobalt crystallites formed by the ultrasound process. In the first preparation 5 g of precursor was used and 3 g of silica was added to the solution (sample C1). In the second preparation both the precursor and the amount of silica were halved so that the cobalt loading on the support was kept the same (sample C2). In the following two preparations (samples C3 and C4) the amount of silica was kept constant while the amount of precursor was again halved. This was done in order to retain enough material that can be conveniently handled for further characterization.

Influence of temperature

Due to the limited amount of the precursor available, more effective use of the remaining cobalt tricarbonyl nitrosyl was made by reducing the concentration of the precursor solutions in these preparations to 1.25 g precursor in 100 ml solvent. This was done similarly to the above procedure.

In order to stabilise the cobalt crystallites formed during the ultrasonication process, 5 ml of oleic acid was added to the precursor/solvent mixture prior to ultrasonication. The temperature of the water bath was adjusted to 35 °C in one preparation and 60 °C in the

following preparation. Ultrasound exposure was set for 2 hours since it has previously been established that an adequate amount of product forms within this period. Furthermore, the shorter ultrasound time was useful for speeding up the preparation process, as well as eliminating possible effects of the declining concentration of precursor with time. Samples T2 and T3 were obtained after the ultrasonication process.

Influence of ultrasound amplitude

These preparations were also performed with solutions containing 1.25 g of precursor in 100 ml n-decane. 5 ml of oleic acid was added to each preparation prior to ultrasound exposure. The ultrasound amplitude was adjusted to 20% in one preparation and 60% for the following preparation. Samples A2 and A3 were obtained after ultrasonication.

2.3 Recovery of material

Use of atmosbag during preparations

In the first experiment where the influence of ultrasonication time was investigated, the ultrasonic probe and reaction vessel was returned to the atmosbag. A small amount of the suspension was extracted using a pasteur pipette and squirted into a politop filled halfway with n-pentane. This politop was closed and left in the atmosbag in order to prevent air from coming into contact with the product. The reaction vessel was closed again and the ultrasound process resumed. Due to the low temperature of the solution and the fact that the extraction process was performed very quickly, it is believed that very little cobalt precursor escaped from the reaction vessel during this process.

The extracted materials were kept inside the atmosbag during the whole experiment. After all four samples were obtained, the politops were opened under argon inside the atmosbag and a small amount of each suspension was dropped onto TEM grids.

In order to prevent excessive oxidation and subsequent sintering of the cobalt crystallites, the samples were gradually exposed to atmosphere by covering the TEM grids inside a petri dish and opening the mouth of the atmosbag slightly. In this way air could enter the atmosbag, but it is believed that the restrictions caused by the slight opening of the atmosbag and the lid of the petri dish was sufficient to limit the rate at which the cobalt

was exposed to oxygen sufficiently. In this way it was ensured that all the samples received the same treatment and were exposed to the same conditions.

A similar procedure was used to obtain TEM samples for the materials formed during the preparations where the temperature and ultrasonic amplitude were varied. In these cases the suspensions formed after each preparation was stored as-is in closed glass containers. After all preparations were completed, small amounts of the suspensions were dropped onto TEM grids, which were simultaneously exposed to air as described above.

Cannulation

In the preparations where the influence of the concentration of the precursor was investigated, the atmosbag was not available for unloading the products. Instead, the product was transferred to a three-neck round bottom flask (see Figure 2-3). The large opening of the round bottom flask was sealed using a septum, while the smaller inlets could be closed either by a screw on cap, or a valve built into the inlet.

The transfer was accomplished without exposing the cobalt products to air. This was done by connecting the side outlet of the reaction vessel to one of the inlets of the round bottom flask using a silicon tube. Argon gas was introduced into the second inlet of the reaction vessel and allowed to flow through the reaction vessel, through the silicon tube into the round bottom flask, exiting at the second outlet of the glass container. This flow was maintained for 30 minutes in order to flush air and unreacted precursor gases from the system. After this period, the n-decane suspension was poured into the round bottom flask by tilting the reaction vessel above the flask. Both ends of the flask were then sealed in order to keep the products in an inert atmosphere.

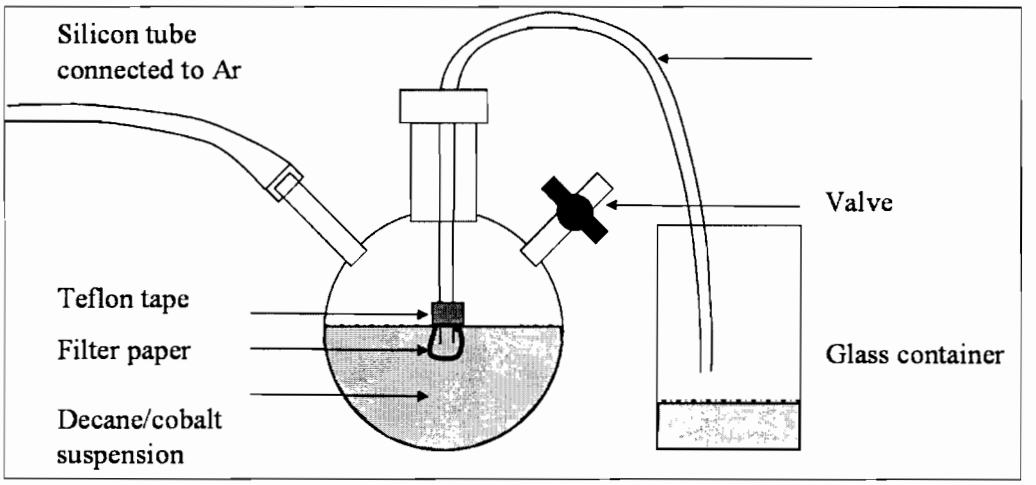

Figure 2-3 Cannulation process to recover the solid product. Argon gas is supplied into the left inlet and exits on the right. The catalyst/n-decane suspension is filtered by the small piece of filter paper on the end of the plastic tube inside the glass container. The liquid exits the container via the tube into the glass beaker.

In order to separate n-decane from the solid cobalt particles, use was made of a process called 'cannulation'. In this process a piece of filter paper is folded and fixed to one end of a thin polymer tube using teflon tape. The other end of this tube is pressed through the septum covering the mouth of the round bottom flask so that the filter paper is situated inside the container. A positive pressure provided by letting argon into the flask through one of the smaller inlets forces the liquid through the filter paper and into the polymer tube, while the solid material stays behind inside the flask.

About 100 ml of n-pentane was poured into one of the inlets of the flask after most of the n-decane had been removed and the filter paper became clogged. The flask was swirled in order to mix the n-pentane with the cobalt particles and the residual n-decane, followed by a second cannulation process. This procedure was repeated five times during which the liquid inside the polymer tube, which initially had a yellow colour, became progressively clearer.

Slow oxidation of the cobalt material was accomplished by closing the one inlet of the round bottom flask only slightly and leaving overnight. This allowed small amounts of air into the container to slowly oxidize the catalyst while most of the n-pentane evaporated.

Finally, the smaller inlets of the flask were completely opened and the flask was heated at a low temperature under argon flow in order to remove all the remaining n-pentane.

2.4 Characterization of materials

For the determination of the crystallite sizes, three different techniques were utilized, viz. Transmission Electron Microscopy (TEM), X-ray Diffraction (XRD) and hydrogen chemisorption. Each technique has its strengths and weaknesses.

- TEM is an accurate technique for measuring single crystallites, gives a very good visual impression of the distribution of crystallite on the support material, and measurements of a number of crystallites gives a crystallite size distribution. However, only a very small fraction of the crystallite population is observed and it is extremely time consuming to obtain a crystallite size distribution.
- XRD, is often used for determining the volume average crystallite size in a specimen, which is derived from a much larger fraction of the crystallite population. However, the technique can only be used for crystalline materials and is practically limited to determination of crystallite sizes in the range of about 2 to 50 nm.
- Hydrogen chemisorption is often applied to yield the average crystallite size and dispersion, but gives no information about the distribution of crystallite sizes.

Although TEM viewing was used extensively in this study to evaluate the cobalt crystallite sizes, the other techniques were also tried. For this reason details of these instruments are also presented here.

2.4.1 Transmission Electron Microscopy

For the unsupported and oleic acid-stabilized materials TEM samples were prepared inside the atmosbag by extracting small amounts of the n-decane/cobalt suspensions from the reaction vessel using pasteur pipettes. A few drops of these suspensions were dropped directly onto TEM grids situated on a piece of filter paper.

The supported materials obtained after the cannulation procedure had already been oxidized. From these materials small amounts of powder were mixed with ethanol in small politops. These mixtures were ultrasonicated in an ultrasonic bath for a few minutes in order to suspend the small particles. After leaving the politops for a further few

minutes in order to let the largest particles settle, small amounts of the suspensions were extracted with pasteur pipettes and dropped onto TEM grids.

TEM images were obtained using a Philips CM200 microscope with a LaB_6 filament as electron source. This microscope was fitted with an Oxford Energy Dispersive X-ray Spectroscopy (EDS) analyzer (used to confirm the identity of the cobalt crystallites), as well as Gatan Image Filter (GIF) that contained a CCD camera for capturing images digitally. The microscope was operated at a 200 kV accelerating voltage.

Cobalt crystallites were measured using the imaging software package Digital Micrograph. Due to the low contrast differences between the cobalt crystallites and the background, the measurements had to be performed manually instead of using the image analysis functions of the software. This has the implication that the projected areas of the crystallites were not measured, but rather their diameters. For an irregularly shaped crystallite the minimum diameter was taken as representing the crystallite diameter. It was estimated that, at a magnification of about 200 000 times (images with a 20 nm scale bar) the measurements introduced an error of about 0.5 nm.

The measurements were grouped into bins of 1nm size intervals in order to obtain the histograms. This bin size was chosen for two reasons. Firstly, a difference in the order of a nanometer or more would be of real interest for this investigation, while smaller differences will probably be of no consequence. Secondly, the errors in the crystallite size measurements were in the order of about 0.5 nm, which should have a relatively small impact on the distribution with the currently selected bin size.

2.4.2 X-ray Diffraction

XRD analyses were performed using a Siemens D500 instrument with a 1.78897 Å cobalt X-ray source and a scintillation detector. The high voltage of the instrument was 40 kV, while the tube current was 40 mA. Analyses were done overnight in order to ensure that spectral peaks can be observed and to improve the signal-to-noise ratio.

2.4.3 Hydrogen Chemisorption

In order to perform this analysis, the passivated catalysts needed to be reduced to the metallic state. In order to identify a suitable reduction temperature, a Temperature Programmed Reduction profile was obtained using an Autochem 2010 instrument. For this analysis 50 mg of material was loaded into a sample tube. A mixture of 10% hydrogen in argon was passed through the sample at a rate of 50 ml(STP)/min, while the temperature was raised at a rate of 10 °C/min from room temperature to about 900 °C. The TPR profile obtained suggested that a reduction temperature of around 280 °C would be sufficient to reduce the catalyst to metallic cobalt in a reasonably short time.

The chemisorption analysis was performed on an ASAP2010 instrument. An amount of 0.2766 g of the passivated supported catalyst was loaded into a quartz tube. Hydrogen gas was passed through the sample for 4 hours at a temperature of 280 °C in order to reduce the cobalt to the metallic state. The material was evacuated for an hour at this temperature and a further 30 minutes at 100 °C in order to remove the remaining hydrogen. The measurement commenced at this temperature, using an equilibration interval of 30 seconds.

3 Results

3.1 Unsupported material

The initial preparations focused on the generation of unsupported material. It was thought at the time that the unsupported material would be easier to characterize. In TEM imaging of alumina-supported cobalt catalysts it is sometimes difficult to distinguish the cobalt crystallites from those of the support material. Another advantage would be that BET surface area analyses could be used to determine the average crystallite size instead of hydrogen chemisorption analyses. In order to perform hydrogen chemisorption analysis, reduction at an elevated temperature is required. This process could induce sintering and hence influence the size of the cobalt crystallites.

3.1.1 Influence of ultrasonication time

This experiment served two purposes. Its primary purpose was to determine whether the crystallite sizes changed as the ultrasonication process continued. Possible factors that may cause such changes are a) the violent collisions between particles may cause interparticle melting where sintering may occur[42], and b) formation of the cobalt crystallites results in the gradual depletion of the cobalt precursor, which may affect the size of newly formed crystallites. Secondly, it was also useful to estimate the rate of formation of the cobalt particles so that a suitable period for ultrasonication could be identified that would yield sufficient material for analysis.

Figure 3-1 shows a low magnification and a higher magnification TEM image of the material obtained after 30 minutes of ultrasonication (sample t0, prepared with 5 g of precursor). The particles typically consist of small crystallites and relatively large holes. Tilting the sample in the microscope reveals the three dimensional nature of this "loose and porous" material which is reminiscent of the links in a chain. The appearance of the crystallites and the lack of flat facetted edges suggest that the material is amorphous. TEM images obtained at higher magnifications did not show any lattice spacings associated with crystalline materials.

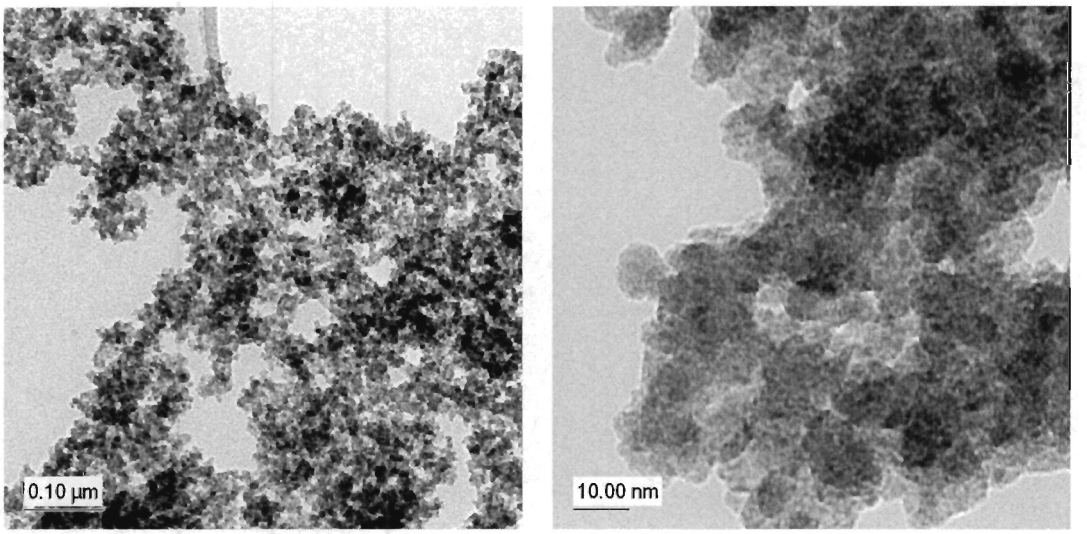

Figure 3-1 Low magnification (left) and higher magnification (right) TEM images of a cobalt particle obtained after 30 minutes of ultrasound exposure.

Suslick et al.[43] prepared Co-Fe alloys with various Co:Fe ratios in a similar manner using iron carbonyl and tricarbonyl nitrosyl cobalt as precursors. From high magnification SEM imaging he describes that "...these materials are porous aggregates of small clusters of 10-20 nm particles." This description fits well with the cobalt material shown in Figure 3-1. A similar description was also given for an unsupported molybdenum carbide material made in a similar fashion. Furthermore, Grinstaff et al.[57] prepared unsupported Fe materials that they described as "porous agglomerates of very small particles."

Low magnification TEM images of the materials collected after 30 minutes (sample t1) and 20 hours (sample t4) of ultrasound exposure are compared in Figure 3-2. The morphologies of the particles and crystallites appear to be similar, while there does not appear to be a significant difference in crystallite sizes. Images from the materials collected after 5 hours (sample t2) and 10 hours (sample t3) are very similar.

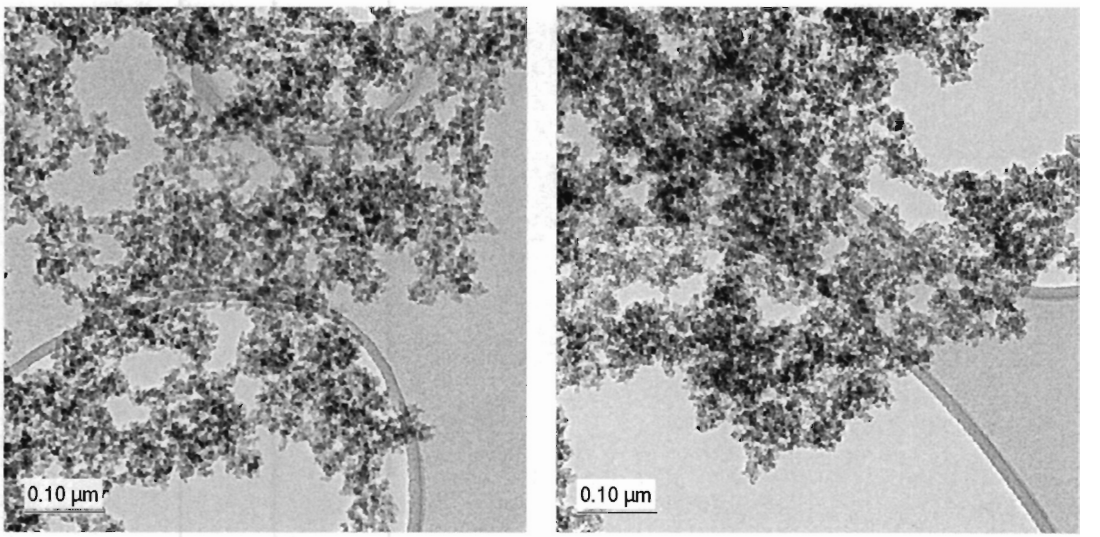

Figure 3-2 TEM images of product obtained after ultrasound exposure for 30 minutes (left) and 20 hours (right).

Figure 3-3 shows the crystallite size distributions of samples t1 to t4 obtained from TEM measurements. Sample t1 (30 minutes of ultrasound exposure) has a broader distribution and a slightly higher number of larger particles than the other samples. Sample t2 (5 hours of ultrasound exposure) has a similar range, but lost some of the components in the larger size range. The distribution of sample t3 (10 hours of ultrasound exposure) appears to have shifted slightly to the left, but with a visible shoulder that overlaps with the range of the previous sample. The distribution of sample t4 (20 hours of ultrasound exposure) is in the same position as sample t3, but without the shoulder.

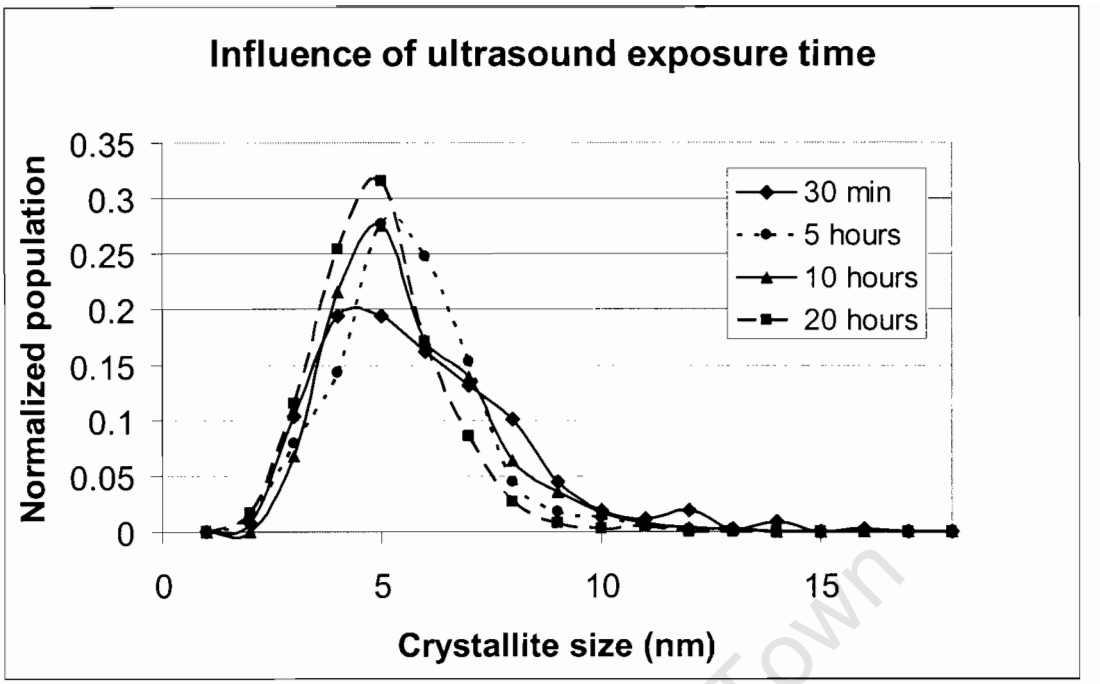

Figure 3-3 Crystallite size distributions obtained after 30 minutes (sample t1), 5 hours (sample t2), 10 hours (sample t3) and 20 hours (sample t4).

Table 3-1 Statistical information of samples obtained after different ultrasound exposure times.

Sample name	Amount of precursor (g)	Number of measurements	Mean (nm)	Std dev (nm)
t0	5	503	5.47	2.3
t1	0.625	427	5.50	2.3
t2	0.625	379	5.13	1.6
t3	0.625	483	5.18	1.7
t4	0.625	409	4.55	1.3

The observations above suggest that there is a trend towards smaller crystallites being formed at longer exposure times. This implies that the concentration of the precursor, which is depleted during the ultrasound process, has an influence on the crystallite size distribution rather than ultrasonication time. Figure 3-4 shows the crystallite size distribution of sample t1 compared to that of sample t0, which was also obtained after 30 minutes of exposure, but was prepared with a larger precursor concentration. Although there are slight differences in the shoulders on the larger crystallite size range, the

distributions are similar in width and there appears to be no significant difference in crystallite size.

The difference between these two distributions is also similar to the differences noted in Figure 3-3. This may suggest that these observed differences are not really significant and that there is really no trend in crystallite size distributions shown in Figure 3-3.

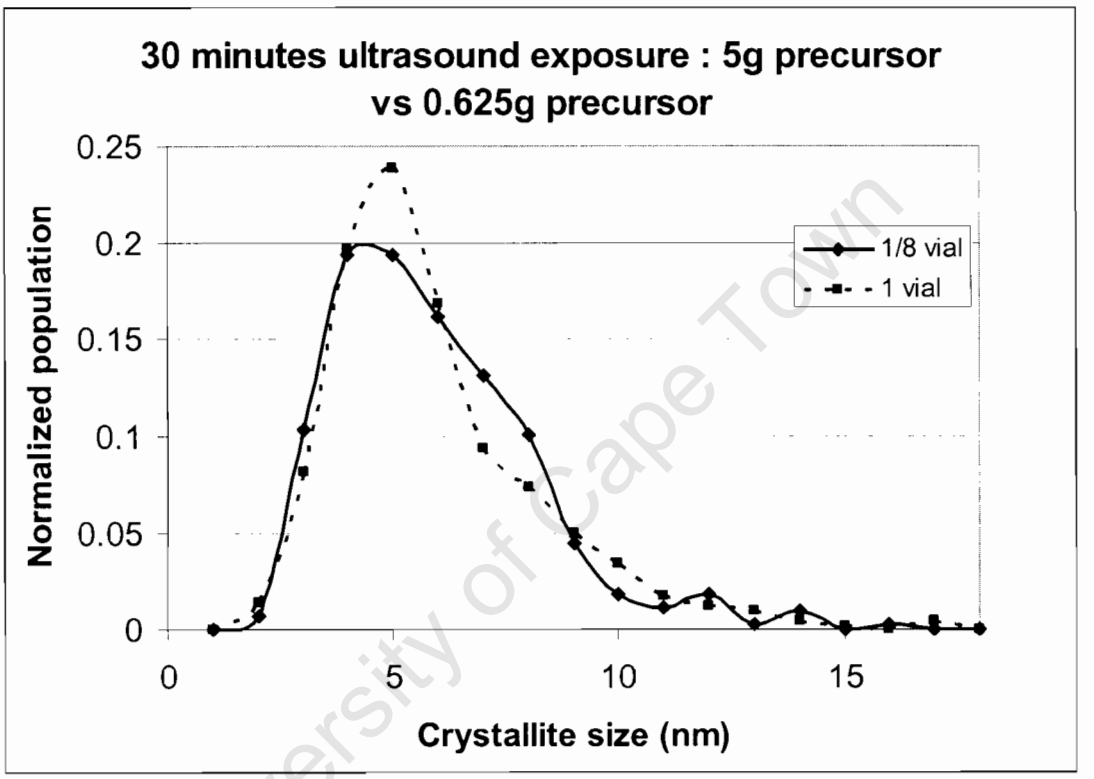

Figure 3-4 Comparison of sample t1 (0.625 g of precursor) to sample t0 (5 g of precursor) after 30 minutes of ultrasound exposure.

The TEM images above show no evidence of temperature induced melting or sintering of the crystallites. Doktycz and Suslick[42] note that very small particles will not have an effect on the shape of the bubbles formed during the ultrasonic process so that microjets will not be formed. As a result acceleration and violent interparticle collisions will not occur. It thus seems that the particles formed in these preparations were too small to affect the shape of the bubbles formed during ultrasonication.

The results above are also significantly different from the observations by Li et al.[60], who reported that the size of their InP particles increased as the ultrasonication time was increased. One explanation that was offered was that the interparticle collisions caused localized heating that led to particle growth. This explanation is a little suspect in the light of the discussion above. They also offered an alternative explanation involving the unstable nature of the surfaces of the formed particles, which then become more stable due to particle growth. However, this effect was not observed in the formation of the cobalt crystallites and cannot be confirmed.

3.1.2 Stability of unsupported material

The images in the previous section show that the crystallites seem to be separate entities that are attached to each other rather than flowing into each other. This suggests that sintering did not occur. This is also supported by the observation that the preparations performed in a similar way (even though at different concentrations, see Figure 3-4) did not show differences in the crystallite sizes.

Grinstaff et al.[57] made similar observations when they noticed that their sonochemically prepared iron powder initially had a surface area of 120 m^2g^{-1} and had a high chemical reactivity. They note that the material sinters at unusually low temperatures and mention that the surface area reduces to <10 m^2g^{-1} after heating at 300 °C.

In the first experiments some attempts have been made to control the rate at which the cobalt oxidized. In one case a dilute mixture of 5% air in argon was bubbled though the suspension while the glass beaker containing the suspension was cooled with dry ice. Figure 3-5 shows TEM images that illustrate the effects of this treatment compared to the normal method of passivation. The large features and the loss of crystallite definition in the image on the right show that this method was not effective in preserving the original crystallite morphology.

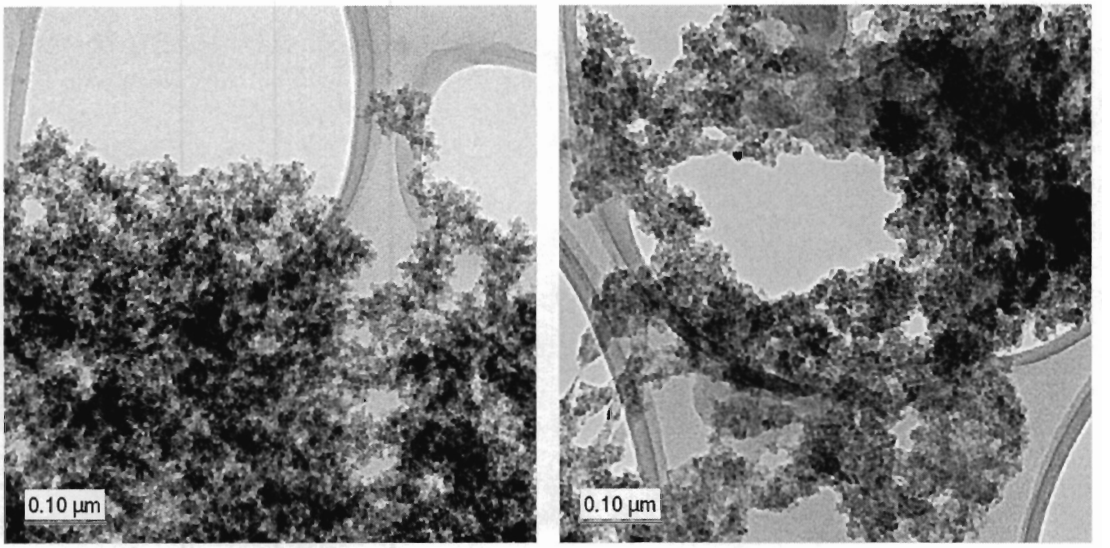

Figure 3-5 TEM image of sample oxidized using conventional method (left) and where a diluted air/argon mixture was bubbled through the suspension while being cooled by dry ice (right).

In another case, the n-decane/cobalt suspension was transferred to a glass beaker and stirred in air. It was thought that air would slowly diffuse into the liquid and come into contact with the crystallites at a limited rate. Figure 3-6 shows TEM images of the result obtained after stirring for 4 hours and 60 hours. Although the image on the left appears to be similar to that shown in Figure 3-2, closer inspection reveals that the crystallites are not so well defined. After stirring for 60 hours, the sample has undergone significant changes and the crystallites are even less well defined. The particles appear somewhat coarser and the crystallites somewhat larger.

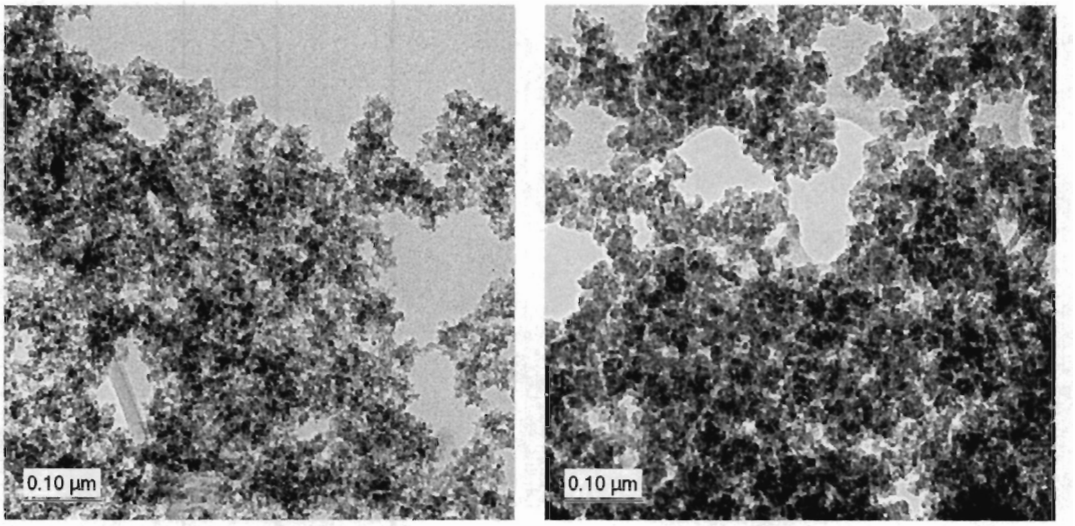

Figure 3-6 TEM images of n-decane/cobalt suspension stirred in air for 4 hours (left) and 60 hours (right).

Another interesting feature of materials prepared without some method of stabilization, is that changes continue to happen. Figure 3-7 shows TEM images of the same material that is shown in Figure 3-6, but viewed again after two weeks. There is a definite change in the morphology of the particles. In the first observation the particles had a visually smaller "grain structure". In the later observation the crystallites seem to have flowed into each other to a larger extent and appeared somewhat larger. The reason for this behaviour is not known. It may possibly have been caused by improper passivation; further oxidation resulted in these changes. It may also be possible that small unsupported particles behave in this way due to the energetic nature of their surfaces.

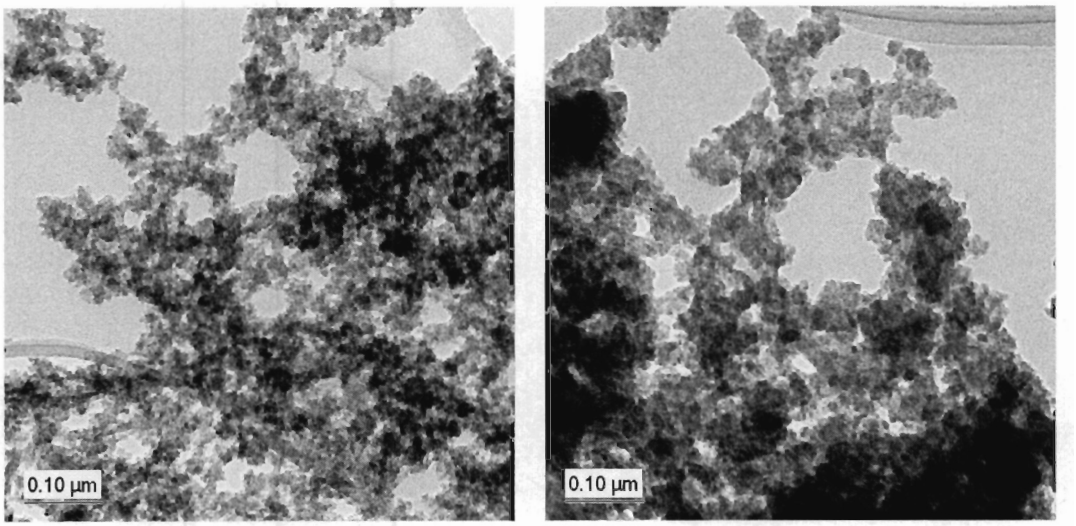

Figure 3-7 TEM images of material obtained two weeks later of material obtained after stirring the suspension for 4 hours (left) and 60 hours (right) in air, viewed two weeks later.

The observations discussed above show that the measurements from unsupported materials are not reliable. The passivation methods are ineffective; even more severely sintered material was seen in preparations other than those shown above. Furthermore, it was also observed that particles within the same sample were often affected differently; some particles showed agglomerations of small crystallites while others showed structures with larger crystallites. The crystallite morphologies also changed with time, thus making it difficult to draw any credible conclusions from the measurement of the crystallite sizes. Despite these complications, it is believed that the results discussed in section 3.1.1 are comparable since the materials were treated in the same way and viewed in the TEM on the same day so that many of the complicating factors have been eliminated.

As a result of the above observations, it was decided to perform further preparations of supported materials using 20 hours of ultrasonication in order to prepare enough material that can be analysed by the various characterization techniques.

3.2 Supported materials

Since the unsupported cobalt crystallites were unstable and prone to sintering, it was decided to stabilize the crystallites on a support material. Silica was chosen as the support

due to the fact that it has a different crystallite structure than that of cobalt, making it easier to distinguish the cobalt crystallites in TEM images.

Figure 3-8 shows two TEM images of the support material obtained at different magnifications. The silica particles are made up of agglomerations of amorphous particles with irregular shapes. The particles are quite transparent with no visible features or speckles.

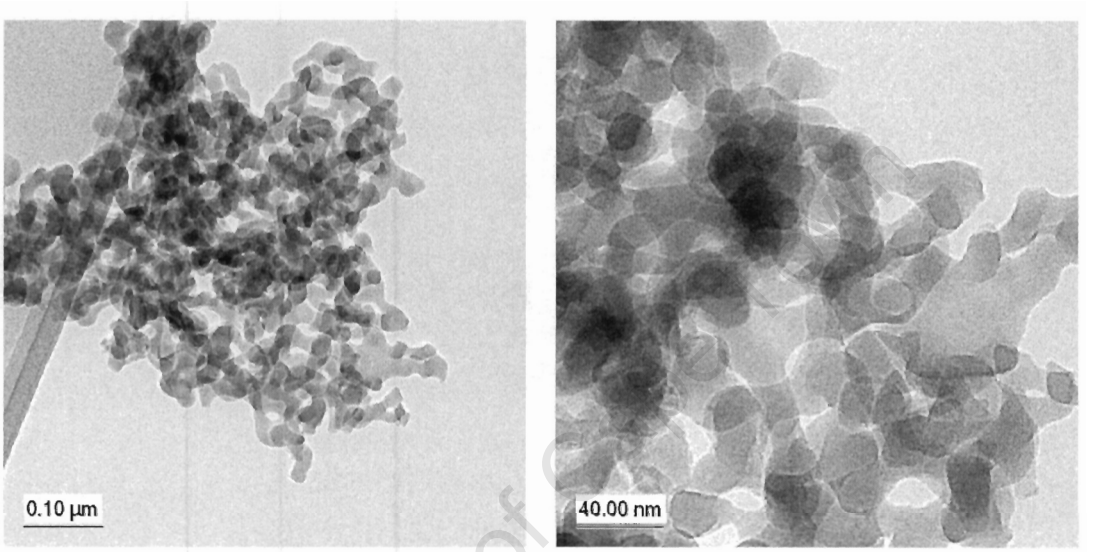

Figure 3-8 TEM images of the clean silica used as support material in this study.

In Figure 3-9 representative TEM images of a silica-supported material (sample C1) are shown. In this preparation 5 g of cobalt precursor was used for the preparation. The cobalt crystallites show up as small dots on the support material and can clearly be discerned by their smaller size and rounded shapes. These speckles appear to be well dispersed on the support, and although they often occur in groups, there does not appear to be excessive clustering. Crystallites that are close to each other and are almost touching are still seen to be separate entities, suggesting that the crystallites were well anchored and no sintering occurred.

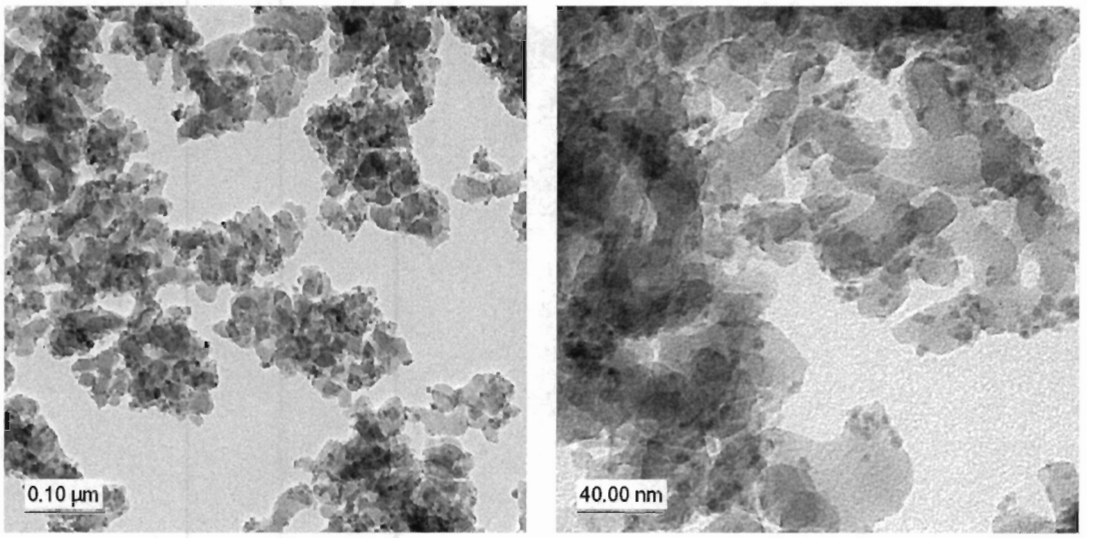

Figure 3-9 Low magnification (left) and higher magnification (right) TEM images of the silica-supported cobalt crystallites obtained using 1 vial (5 g) of precursor.

The cobalt crystallites shown above have sizes that range from less than 1 nm to about 6 nm, with a mean crystallite size of just below 3 nm. Suslick et al.[43] produced a silica-supported iron catalyst by ultrasonic irradiation of iron pentacarbonyl in the presence of silica gel. This resulted in iron crystallites that were highly dispersed on the silica surface and ranged in size from 3-8 nm, which is only slightly different from that of the cobalt preparation.

3.2.1 Influence of precursor concentration

One would intuitively reason that a higher concentration of cobalt precursor would lead to a higher influx of cobalt-containing vapour into the bubbles as they grow during the expansion and contraction cycles. This would lead to a larger amount of the precursor molecules within the bubbles at the stage where they collapse, which should result in larger particles.

In order to investigate this possibility, solutions with different precursor concentrations were prepared as outlined in the experimental section. A summary of the precursor amounts and support amounts is again provided in Table 3-2.

Figure 3-10 to Figure 3-13 show representative low magnification and higher magnification TEM images of the prepared materials. The crystallites appear very similar

in morphology in each of the images and no observable sign of sintering is observed. Visually no observable differences between the samples can be seen.

Table 3-2 Statistical results of crystallite size distribution determinations

Sample name	Amount of precursor (g)	Amount of support (g)	Number of measurements	Mean (nm)	Std dev (nm)
C1	5	3	206	2.56	1.04
C2	2.5	1.5	314	2.76	1.05
C3	1.25	1.5	385	2.85	1.03
C4	0.625	1.5	209	2.18	0.77

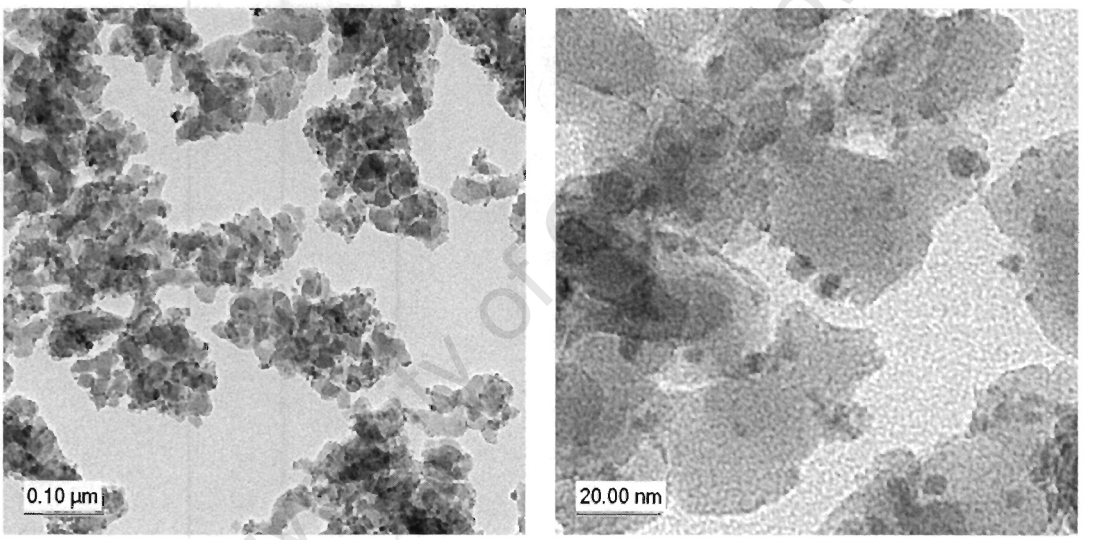

Figure 3-10 Low magnification (left) and higher magnification (right) TEM images of the supported material prepared with 5 g of precursor

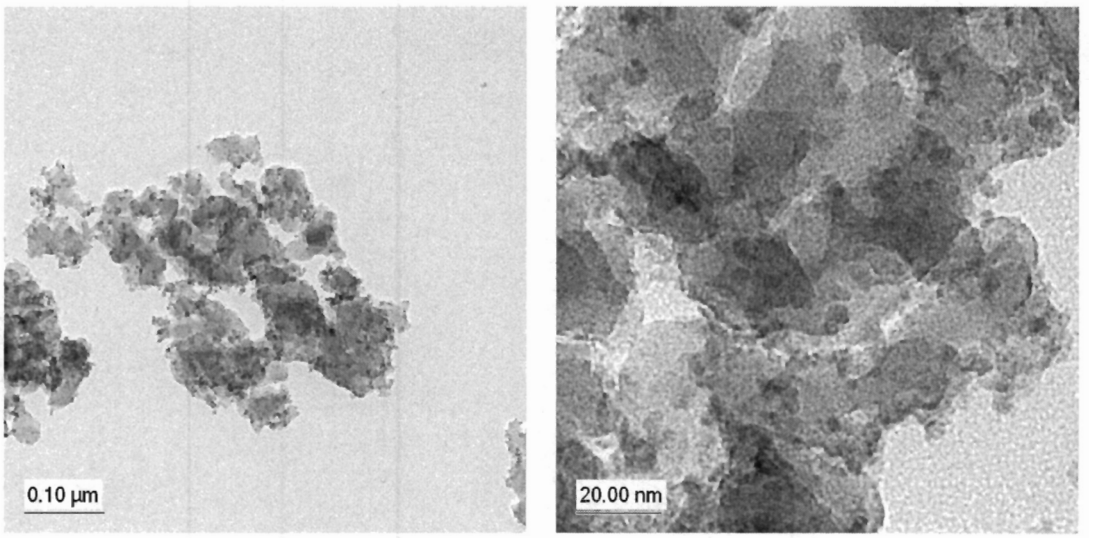

Figure 3-11 Low magnification (left) and higher magnification (right) TEM images of the supported material prepared with 2.5 g of precursor

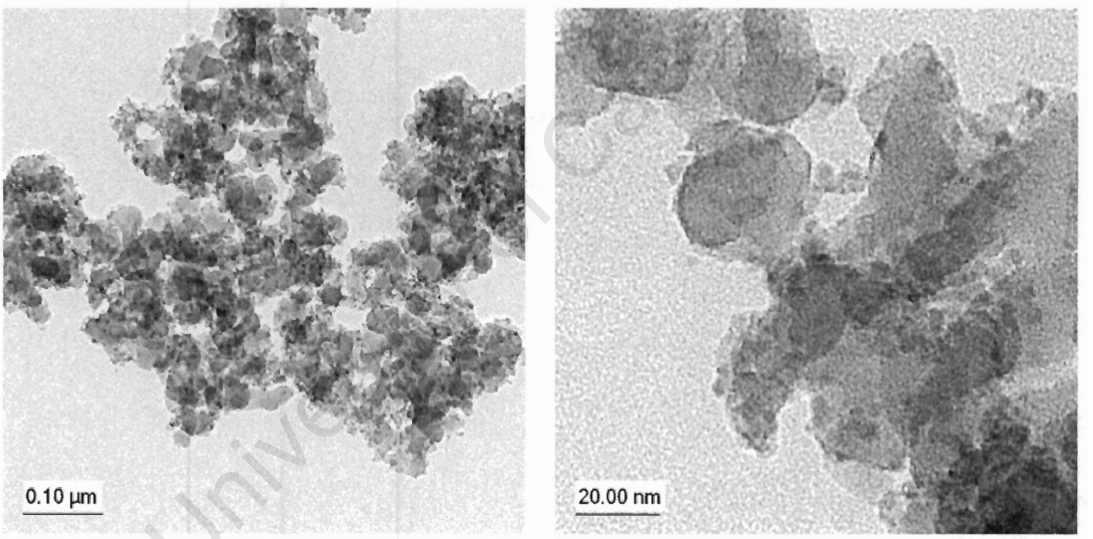

Figure 3-12 Low magnification (left) and higher magnification (right) TEM images of the supported material prepared with 1.25 g of precursor

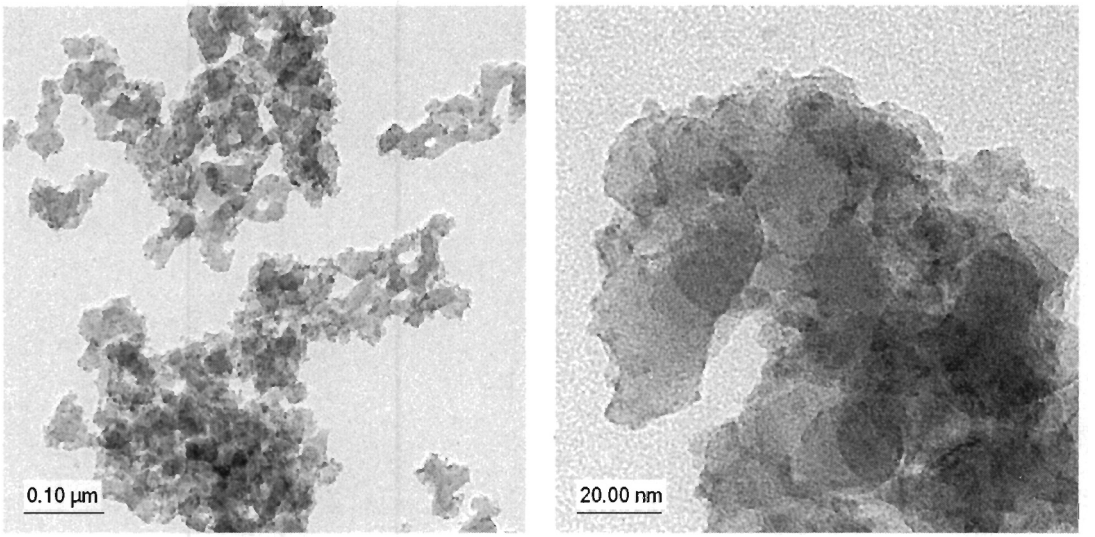

Figure 3-13 Low magnification (left) and higher magnification (right) TEM images of the supported material prepared with 0.625 g of precursor

Figure 3-14 compares the crystallite size distributions of all four samples as obtained by measuring the crystallites in TEM images. The mean and standard deviation of each distribution are provided in Table 3-2. According to Figure 3-14, the crystallite size distributions of samples C2 and C3 are very similar, while those of samples C1 and C4 are shifted slightly to the left. However, the positions of the distributions do not gradually change as the precursor concentration increased. This lack of a trend suggests that there is no link between the crystallite size and the precursor concentration.

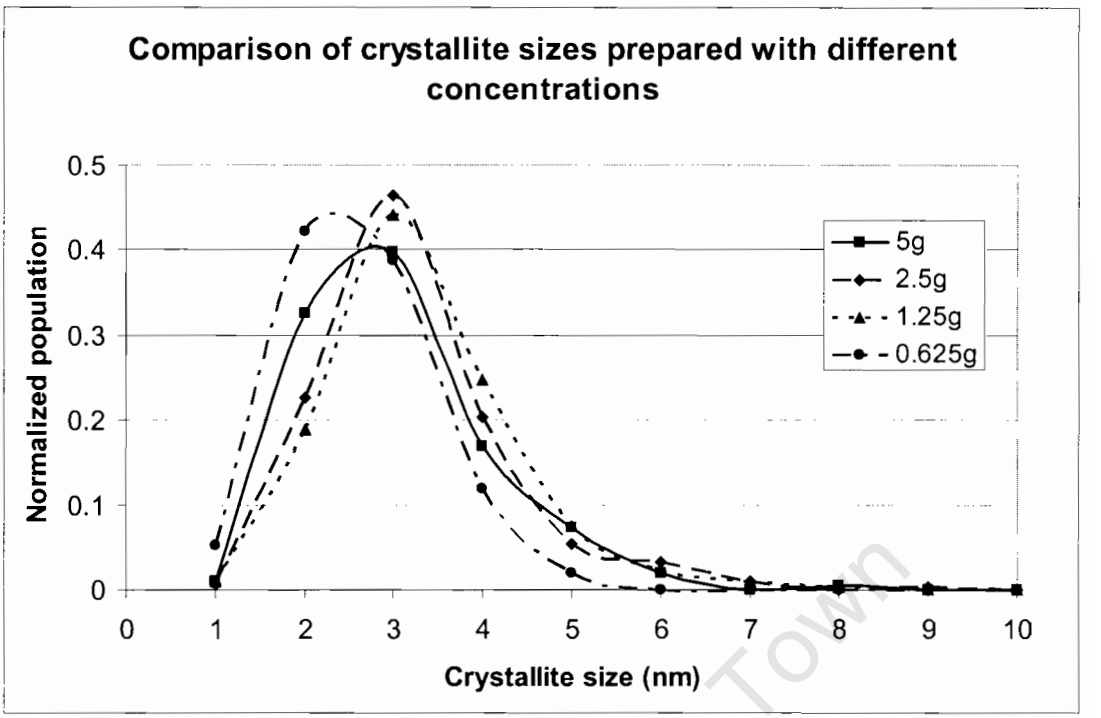

Figure 3-14 Comparison of the crystallite size distributions of the materials prepared with the indicated precursor concentrations.

In this experiment the precursor concentration was reduced by a factor of 8. If one assumes that the volume of the cobalt in the collapsing bubble will also decrease by this factor and that the resulting crystallites are spherical, then the crystallite diameters measured in the TEM images, should decrease by a factor of 2. This is certainly not observed in the above results. It may be possible that the amount of precursor inside the bubbles are decreased by a factor of less than 8, but one would still expect to see a trend as the concentration is reduced.

3.2.2 Hydrogen chemisorption analysis

A prerequisite for hydrogen chemisorption analyses is that the samples should be free from residual carbonaceous material such as the solvent in order to protect the instrumentation. The residual n-decane can be removed by heating the powder to the boiling point of the solvent (174 °C). It was initially feared that heating at this temperature may initiate sintering of the cobalt crystallites. However, TEM images of a sample of the supported material that was heated at this temperature overnight did not show any significant impact on the crystallite sizes. It was also noted that the smaller

crystallites seen in the original material were still present in the heated material, lending further support to this conclusion.

The hydrogen chemisorption process requires that the metal crystallites first be reduced to the metallic state. It was previously attempted to circumvent this reduction step by inserting a supported material that has been washed with n-pentane into the analysis tube under argon inside the atmosbag. This tube was then blocked at both ends using rubber stoppers. However, the resulting adsorption profile indicated almost no adsorption of hydrogen. Although care was taken to prevent exposure to atmosphere, it is suspected that the sample re-oxidized either inside the atmosbag due to some remaining oxygen, or while the tube was connected to the instrument where brief exposure to atmosphere could not be prevented.

The reduction process has to take place at a temperature that is high enough to sustain a reasonable rate of reduction, but also as low as possible to minimize the possibility of sintering. In order to identify a suitable temperature for this reduction, a Temperature Programmed Reduction profile was obtained (see Figure 3-15). It was decided to perform the reduction at 280 °C for 4 hours since the rate of hydrogen consumption is somewhat below the maximum at this temperature.

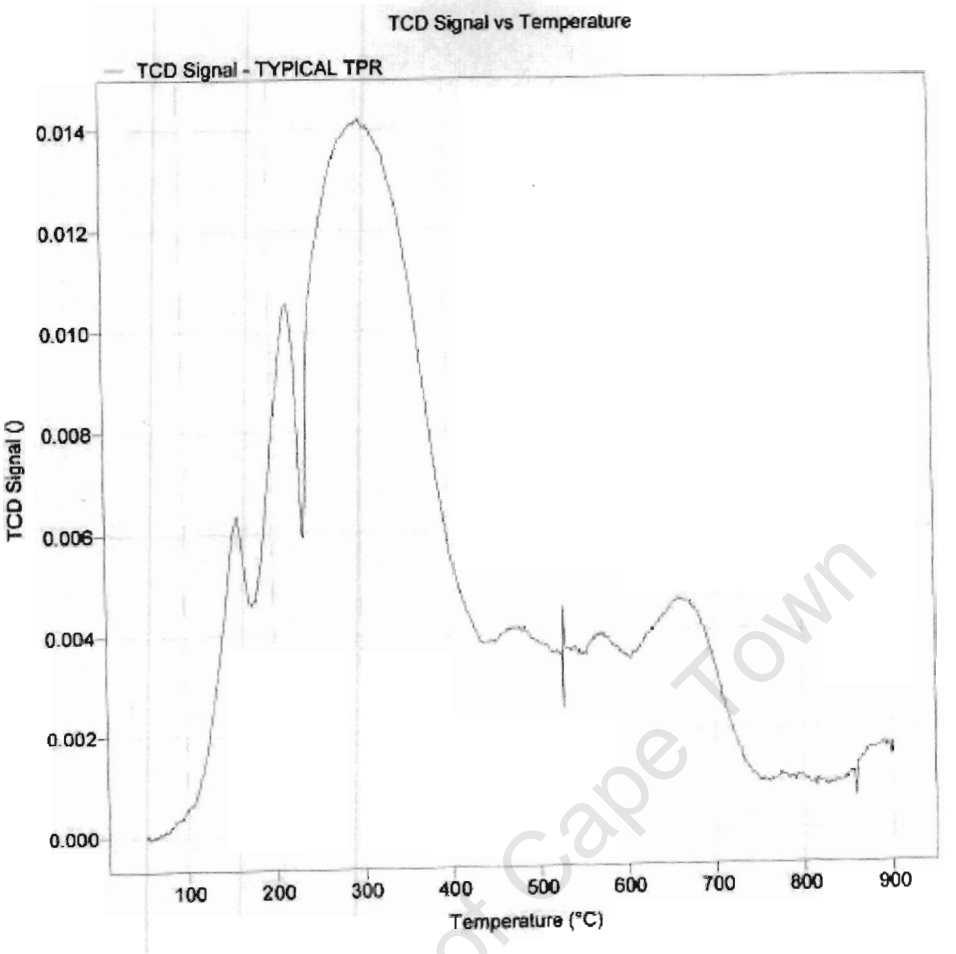

Figure 3-15 Temperature Programmed Reduction profile of the supported material (sample C1).

It is interesting to note that the TPR profile in Figure 3-15 is different from the profile of pure Co_3O_4 that was reported by van Steen et al.[67]. They found that unsupported Co_3O_4 has reduction peaks with maxima at around 260 °C and 350 °C. After impregnating cobalt onto silica materials with increasing surface area, they noticed that the first peak remains at a similar temperature (around 290 °C), while the second peak decreases in intensity as the surface area is increased. Simultaneously, broad features at higher temperatures form that are ascribed to species that are difficult to reduce.

The ultrasonicated sample above has peaks occurring at 150 °C, 220 °C, 300 °C, as well as a broad feature that extends from about 400 °C to 750 °C. The broad feature can probably also be ascribed to interaction with the silica support forming cobalt silicate species that are difficult to reduce. It is not certain why there are three peaks in the lower

temperature region. At the time of this analysis, the amount of hydrogen consumed could not be retrieved from the controlling computer, making further interpretation of the profile difficult. It is worthwhile to note, however, that these initial three peaks occur at temperatures that are significantly lower than those of pure Co_3O_4. It is not certain why this occurs, but one can speculate that the amorphous nature of the cobalt crystallites may make them more reactive.

Figure 3-16 shows the hydrogen chemisorption profile for sample C1. The initial adsorption profile (indicated by the triangular data points) shows a steep initial increase at low pressures, followed by a relatively flat region at higher pressures. This is typical of Langmuir adsorption, described by :

$$\frac{V}{V_m} = \frac{K \cdot P_{H2}^{\frac{1}{2}}}{1 + K \cdot P_{H2}^{\frac{1}{2}}}$$

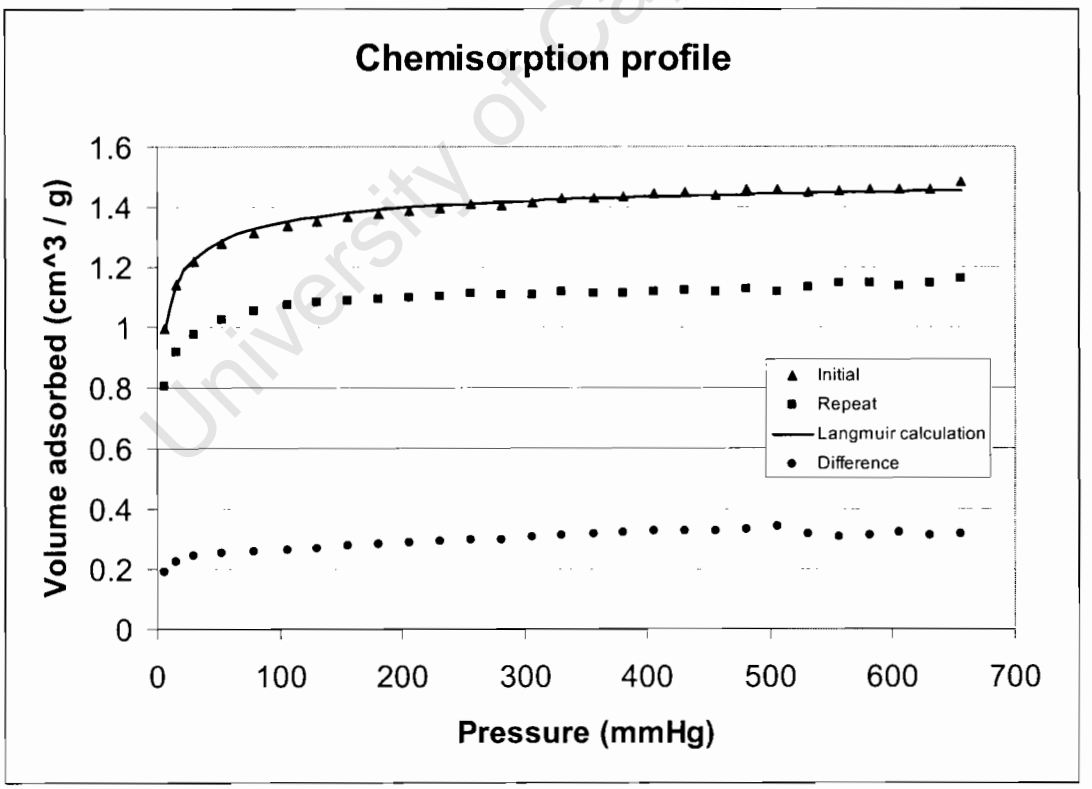

Figure 3-16 Hydrogen chemisorption profile for the supported material (sample C1). The solid line represents the fitted Langmuir isotherm.

This equation can be linearised in order to determine K and V_m from the measured data points, yielding K = 0.7365 $mmHg^{-1/2}$ and V_m = 1.530 cm^3(STP)/g. The solid line shown in Figure 3-16 shows that the Langmuir model fits the data very well. Calculations from the volume of hydrogen adsorbed yielded an average crystallite size of about 8.3 nm (see Appendix).

It must be noted that, for the above calculation, the amount of cobalt in sample C1 had to be determined using ICP analysis. This was necessary since it was not known how much cobalt actually was converted into crystallites and actually ended up on the support. According to the ICP analysis results, the cobalt content in sample C1 was 6.7 mass%. In the synthesis of the catalyst 1.7 g of cobalt was loaded (corresponding to 3 g $Co(CO)_3(NO)$ and 3 g SiO_2). Thus, the yield of cobalt crystallites was ca.12-13%.

In order to ensure that the hydrogen chemisorption method indeed measured the correct average crystallite size and that the crystallites were not altered by the reduction process, TEM images were obtained of the material collected from the chemisorption equipment after the analysis. In Figure 3-17 a representative TEM image of this material is compared to an image of the original material. The crystallites in the reduced material are noticeably larger than the crystallites in the original material. Although some small crystallites still occur in the reduced material, there are no groups or clusters of smaller crystallites present anymore, which suggests that these clusters must have merged into larger crystallites.

Figure 3-18 compares the crystallite size distributions of these two samples and confirms that sintering has indeed taken place during the reduction step. For this evaluation a total of 248 crystallites have been measured for the sample obtained after chemisorption. The mean crystallite size was determined as 4.35 nm (σ = 1.94 nm), which is significantly larger than the mean size of 2.56 nm measured for the sample before the analysis. This value is, however, significantly smaller than the value of 8.3 nm obtained using hydrogen chemisorption.

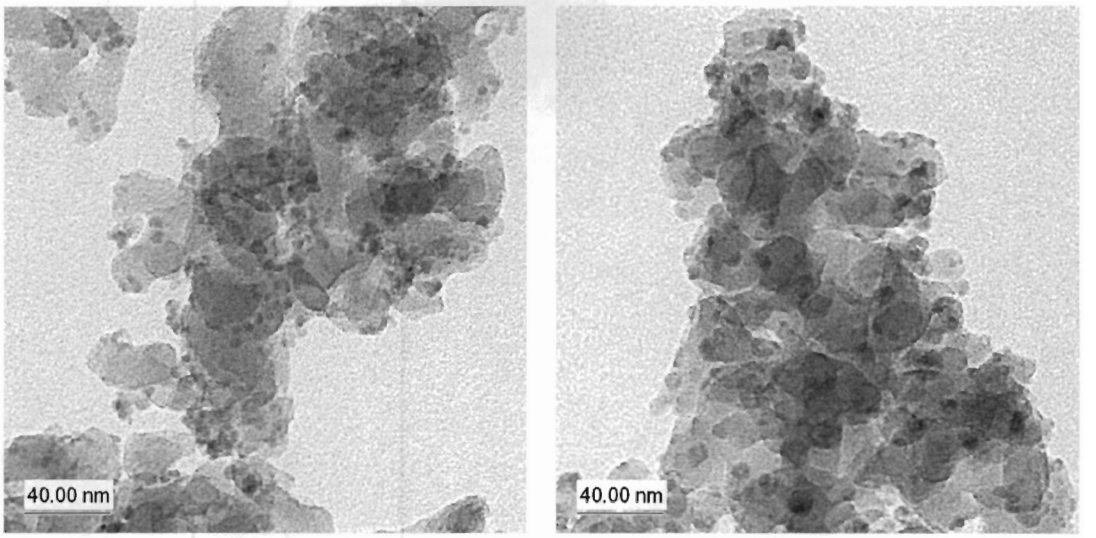

Figure 3-17 TEM images of the supported material before (left) and after (right) the chemisorption analysis.

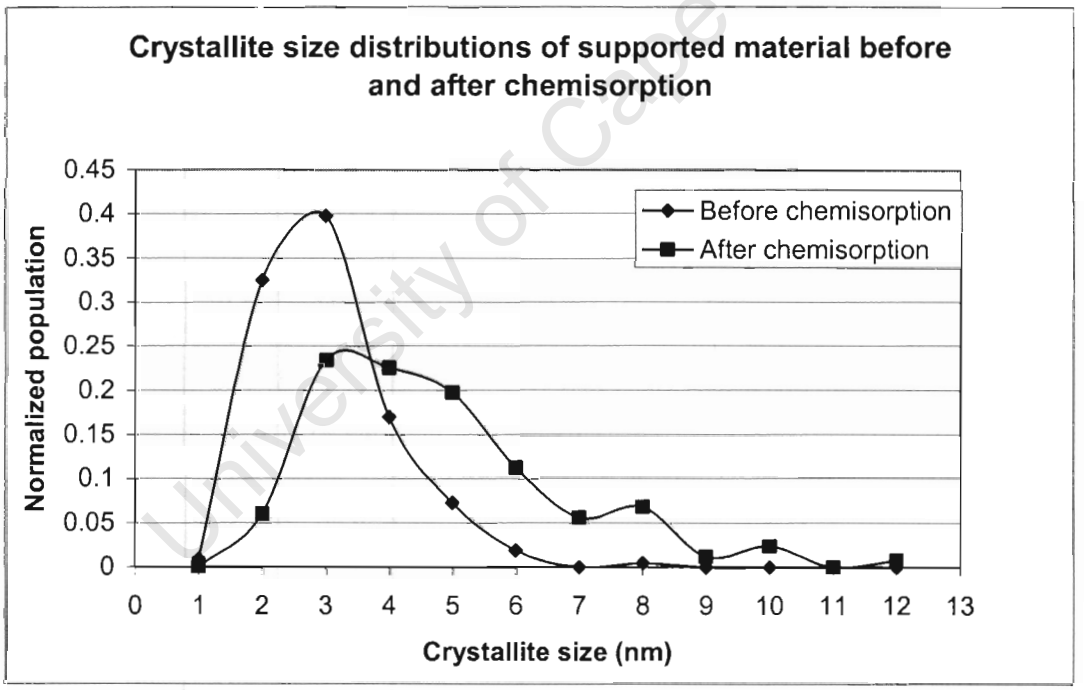

Figure 3-18 Comparison of the crystallite size distributions of the supported material before and after the hydrogen chemisorption analysis.

Hydrogen chemisorption determines the area average of the crystallite sizes, whereas the TEM analyses determined the number average. In order to make a more direct comparison, the crystallite size distributions of the materials obtained before and after the chemisorption analysis was converted to their area distributions. This is shown in Figure 3-19.

In this kind of distribution the larger particles make a significantly larger contribution to the area than the smaller ones. As a result the distribution graphs appear to shift somewhat to the right, while features on the larger particle size are more pronounced. The area average of the crystallite sizes was now calculated as about 6.4 nm, which is closer to the value of 8.3 nm determined by hydrogen chemisorption.

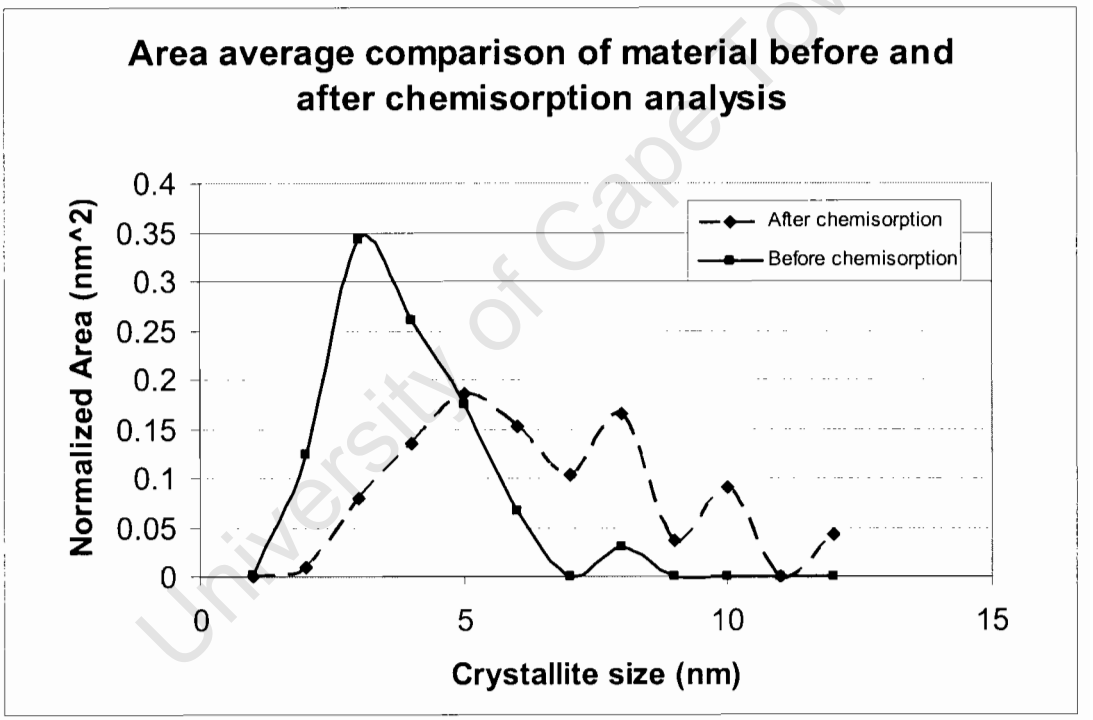

Figure 3-19 Comparison of the area size distributions of the supported material before and after the hydrogen chemisorption analysis.

One must also keep in mind that the reduction conditions used prior to the chemisorption analysis may not have been sufficient to reduce all the cobalt in the sample. The TPR profile in Figure 3-15 shows that there are species present in the sample that are difficult

to reduce. This would lead to an overestimation of the crystallite size, which may account for the discrepancy between the TEM and chemisorption results.

Due to the fact that the reduction process of the chemisorption analyses had a significant influence on the cobalt crystallite sizes, it was concluded that hydrogen chemisorption analyses will not determine the average crystallite sizes of these materials accurately. Consequently, analyses using this method were not further pursued.

3.2.3 X-ray diffraction analysis

It must firstly be noted that an XRD analysis of an unsupported material showed no peaks that could be attributed to a crystalline cobalt phase. This is similar to the observations by Suslick et al.[43] , who found that the iron prepared in their ultrasonication preparations was amorphous, as determined by using differential scanning calorimetry (DSC), XRD and electron beam diffraction. This was as a result of the tremendously high cooling rate experienced after the bubble collapse. The DSC analysis performed by Suslick and co-workers showed that crystallization of the iron particles takes place at 335 °C.

Shafi et al.[44] also used ultrasonication to produce nano-sized amorphous Fe-Ni-Co alloys that were smaller than 10nm. Similarly, Koltypin et al.[68] prepared amorphous tungsten oxide nanoparticles by ultrasonicating $W(CO)_6$ in diphenylmethane. From the lack of peaks in the XRD spectrum, it is thus reasonable to assume that the cobalt crystallites are also X-ray amorphous.

It is interesting to note at this point that not all materials produced by ultrasonication methods are necessarily amorphous. Li et al.[60] found that their InP nanocrystals prepared by ultrasonication of nobel metal complexes in water were well crystallized.

The cobalt material prepared in this study was subjected to a temperature of 280 °C for 4 hours during the reduction process of the chemisorption analysis. It was thought that the material obtained after the chemisorption analysis may be sufficiently crystalline to show diffraction peaks that can be used to determine the average size of the cobalt crystallites. The resulting XRD profile (Figure 3-20) shows one large peak and only two clear peaks at 2θ angles of 43 ° and 52 °. The broad peak is most probably due to the amorphous

silica in the sample, as confirmed by performing an XRD scan of the support material without cobalt. The other two peaks can possibly be assigned to Co_3O_4 (shown by the peak identification lines), although this is not entirely certain as not all the peaks of this phase show up on the XRD profile.

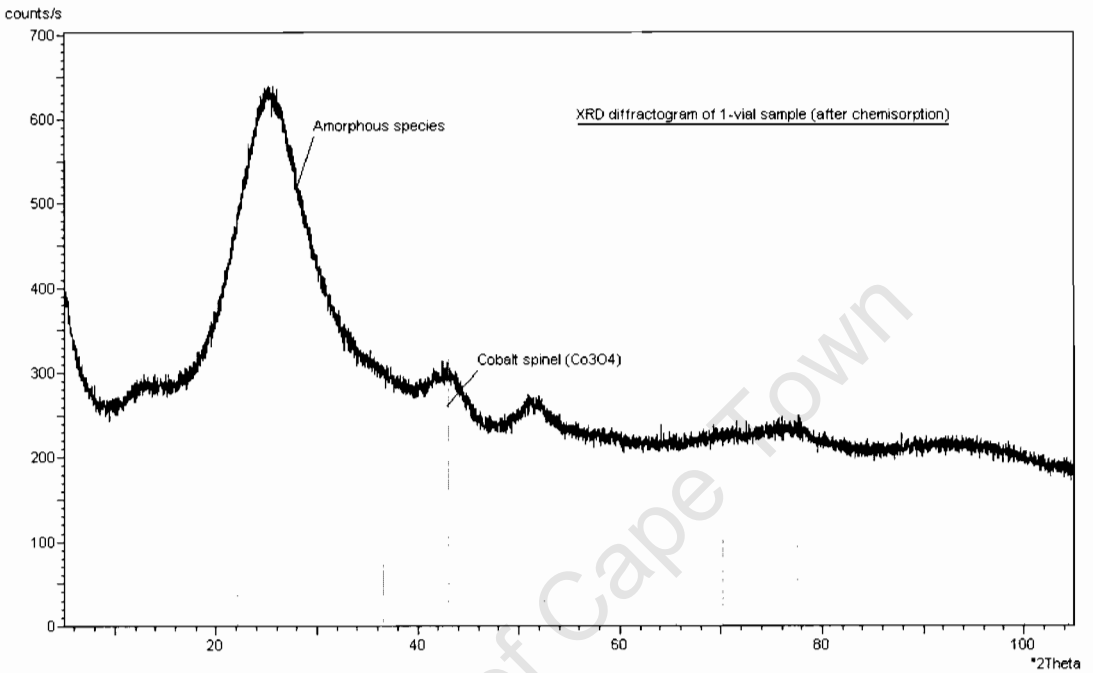

Figure 3-20 XRD profile of material obtained after the chemisorption experiment.

The absence of well-defined peaks in this profile can possibly be attributed either to persistent poor crystallinity of the cobalt, or to the small size of the crystallites. It was not possible to perform a Rietveldt refinement of the profile in order to accurately determine the average size of the crystallites. However, assuming that the peak indicated in Figure 3-20 is indeed cobalt spinel, use of the Scherrer equation to calculate the average crystallite size from the peak width yielded a size of around 6 nm.

Since XRD measures the volume average, the TEM measurements were converted to a volume size distribution, shown in Figure 3-21. The volume average crystallite size was calculated from this distribution as 7.3 nm, which corresponds quite well with the XRD value.

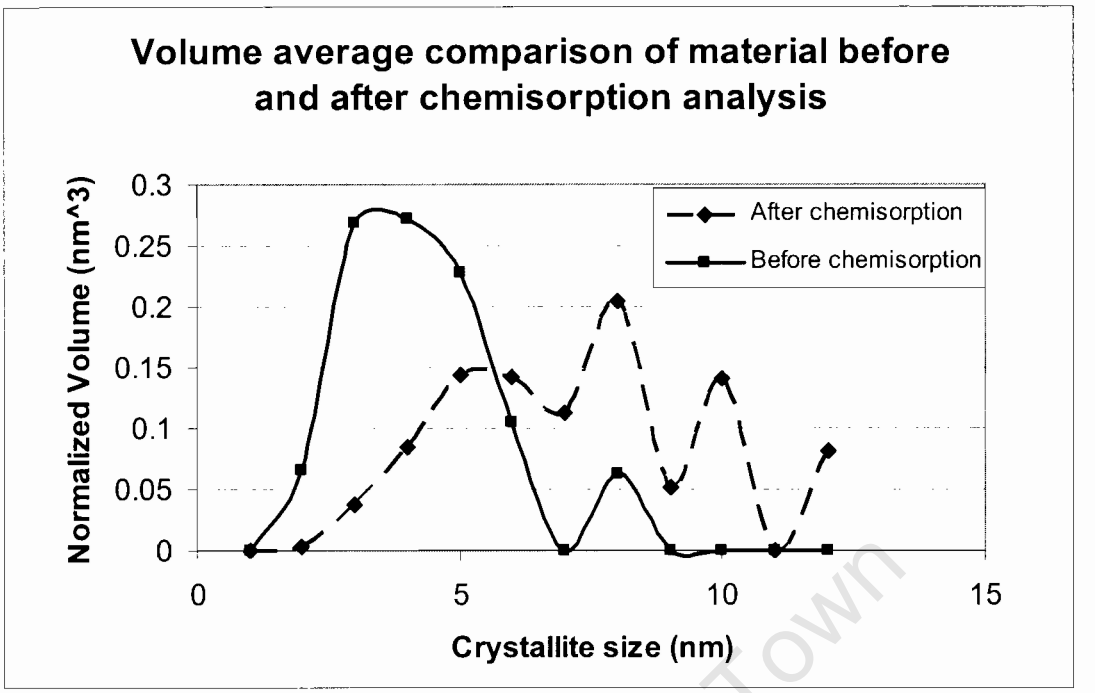

Figure 3-21 Comparison of the volume size distributions of the supported material before and after the hydrogen chemisorption analysis.

Despite the good correlation with the TEM results, this technique was not further utilized due to the fact that the material had undergone changes during the reduction process.

3.3 Materials stabilized by oleic acid

Since the previous attempts of characterizing the formed materials using other techniques were unsuccessful in reliably determining the average cobalt crystallite size, it was decided at this point to only use TEM for characterization. Furthermore, stabilization of the cobalt crystallites by forming colloidal particles, was investigated. For this purpose 5 ml of oleic acid was added to the initial solvent and precursor mixture.

Figure 3-22 shows TEM images obtained from such a stabilized sample after 20 hours of ultrasonication. In this preparation one full vial (5 g) of precursor was used (sample T1). The images show cobalt crystallites in the range of about 1 to 5 nm, separated from each other by a carbonaceous matrix. The small sizes and discrete nature of the crystallites suggest that these crystallites are the primary product from the ultrasonication process and not the product of sintered material.

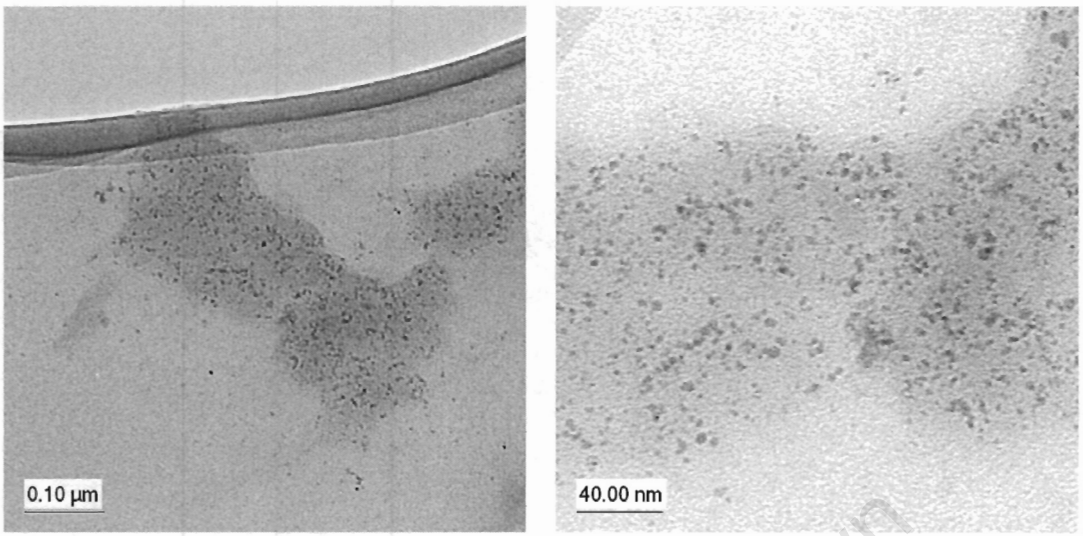

Figure 3-22 Low magnification (left) and higher magnification TEM images of the oleic acid-stabilized cobalt crystallites obtained after 20 hours (5g of precursor).

Since it was now not necessary to produce larger quantities of material, the precusor/solvent mixture was only exposed to ultrasound for 2 hours. This considerably speeded up the rate at which materials could be prepared, but also had the added advantage that any possible effects that prolonged ultrasound exposure may have on the crystallite sizes were eliminated.

3.3.1 Influence of temperature

Figure 3-23 and Figure 3-24 show TEM images of the materials obtained at temperatures of 35 °C (sample T2) and 60 °C (sample T3). Although these preparations were performed with 1.25 g of precursor as well as a shorter ultrasound exposure time, the results discussed previously showed that these differences should not have an influence on the crystallite size distributions. These materials can thus be directly compared to sample T1 (Figure 3-22).

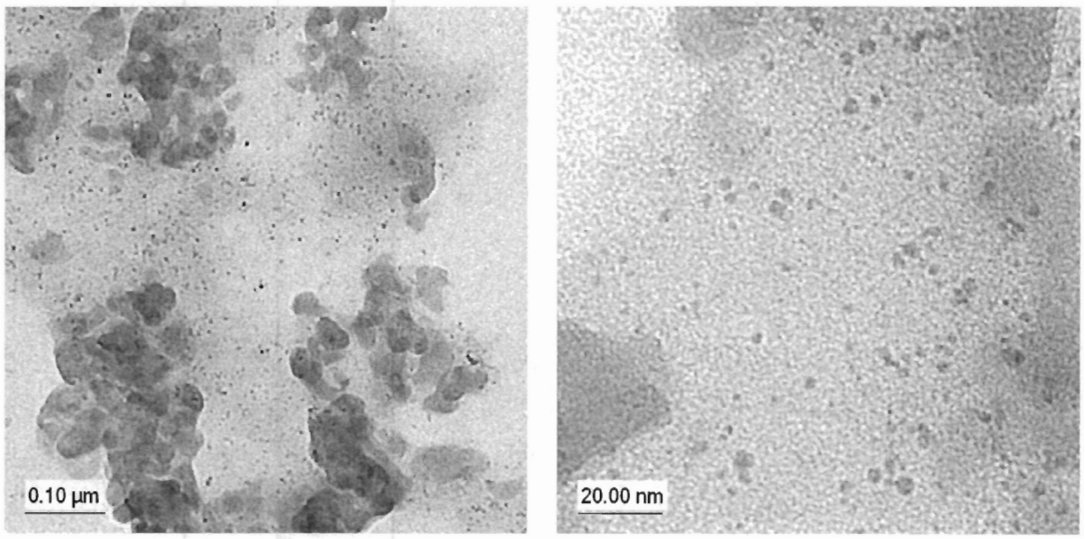

Figure 3-23 Low magnification (left) and higher magnification TEM image of material prepared at a temperature of 35 °C.

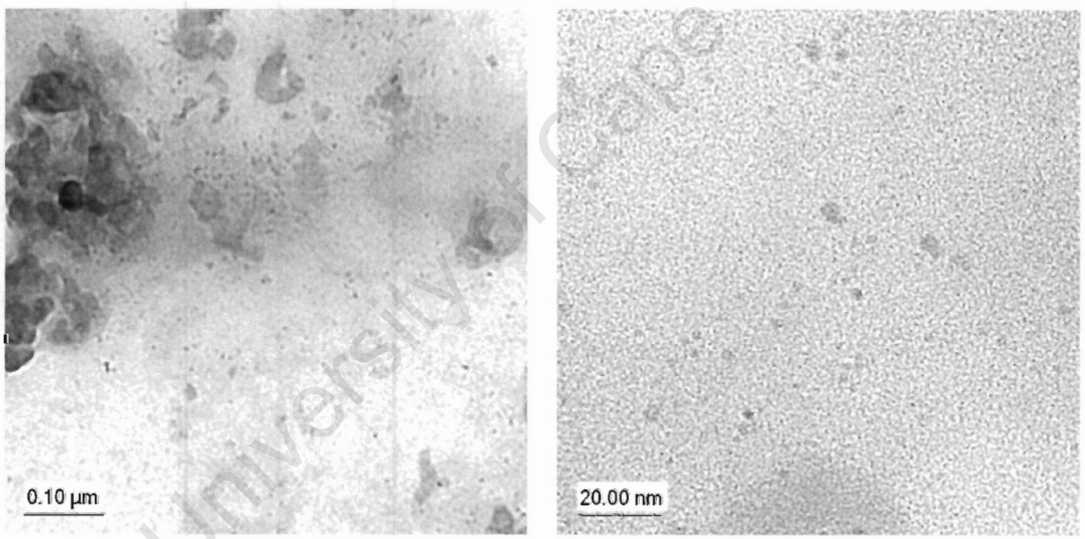

Figure 3-24 Low magnification (left) and higher magnification TEM image of material prepared at a temperature of 60 °C.

The TEM images do not show a noticeable difference in crystallite size between the three different materials. Figure 3-25 shows a comparison of the crystallite size distributions obtained from measuring a large number of crystallites from different regions on each sample. The results of these measurements are summarized in Table 3-3. These results confirm that, within this temperature range, the crystallite size is not significantly affected by the temperature of the precursor/solvent solution. Since sample T1 was

prepared with a higher precursor concentration than samples T2 and T3, the fact that the crystallite size is not influenced by the precursor concentration is again supported.

Table 3-3 Materials prepared at different temperatures.

No	Temperature (°C)	Precursor concentration (g)	Number of measurements	Mean (nm)	Std dev (nm)
T1	10	5	651	2.00	0.74
T2	35	1.25	767	1.86	0.64
T3	60	1.25	675	1.83	0.70

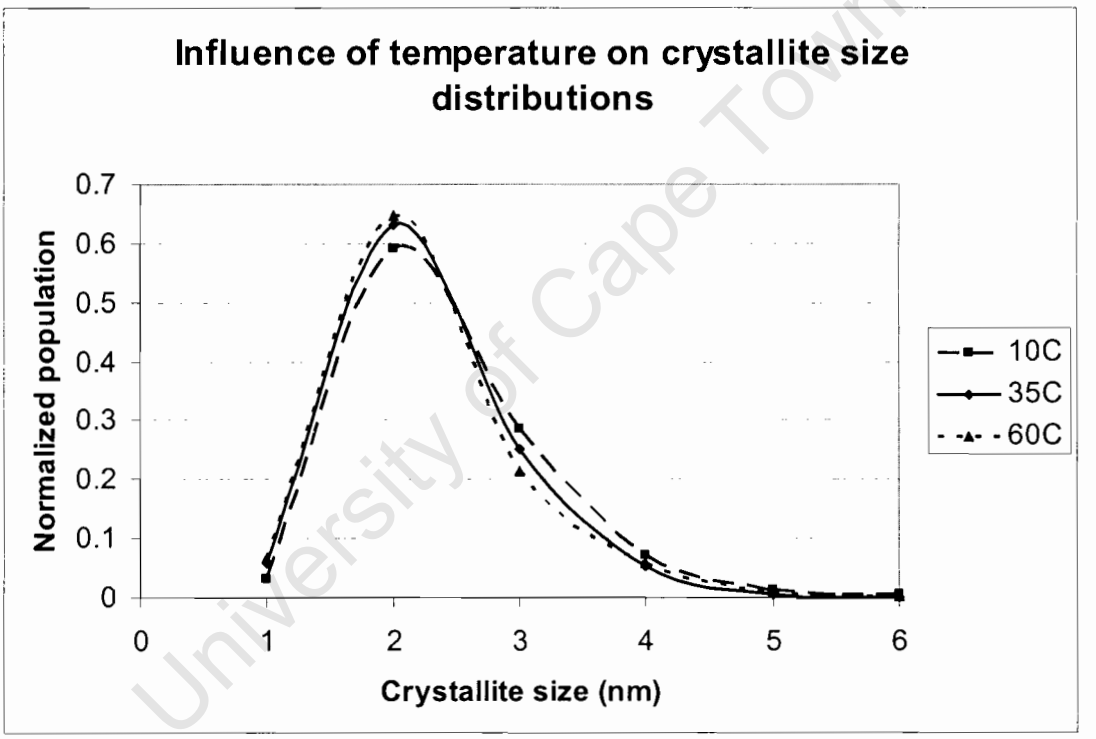

Figure 3-25 Comparison of the crystallite size distributions of materials prepared at different temperatures.

Didenko et al.[58] found that the sonoluminescence intensity in water diminished with an increase in temperature (10 - 75 °C). Shafi et al.[54] states that the concentration of the precursor in the bubble increases linearly with its vapour pressure, thereby increasing the ultrasonication rate. This was confirmed by Suslick et al.[38] who varied the vapour pressure of iron pentacarbonyl in alkane solutions by increasing the solution temperature

and showed that the sonochemical rate coefficient depends linearly on the vapour pressure of the metal carbonyl.

This apparent contradiction can perhaps be explained by the fact that the boiling temperature of water is somewhat lower than that of the decalin or alkanes used in the other two studies. The amount of water vapour inside the bubble thus increases significantly as the temperature is raised, which has a detrimental effect on the bubble implosion intensity[57]. In the study by Suslick et al., care was taken to keep the vapour pressure of the solvent constant.

This can perhaps also explain the reason why the solution temperature did not affect the size of the cobalt crystallites. The boiling point of n-decane is far above the temperature range investigated in this study, so that the amount of n-decane vapour inside the collapsing bubbles probably did not increase significantly. However, one should keep in mind that the increase in precursor concentration also did not influence the cobalt crystallite size. It can also be noted that changes in other properties, such as viscosity and surface tension, also did not seem to affect the size of the cobalt crystallites significantly.

3.3.2 Influence of ultrasound amplitude

In this experiment it was attempted to influence the size of the cobalt crystallites by varying the amplitude of the ultrasound. As mentioned in the Introduction section, Li-yun et al.[59] noticed that size of their hydroxyapatite particles decreased at higher power settings of the ultrasound instrument, although no explanation for this observation was given.

Figure 3-26 and Figure 3-27 show representative TEM images of the products obtained at amplitude settings of 20% and 60% (samples A1 and A2 respectively). The crystallite sizes appear very similar and are also in agreement with the material prepared with an ultrasound amplitude setting of 40% (sample T1) shown previously in Figure 3-22.

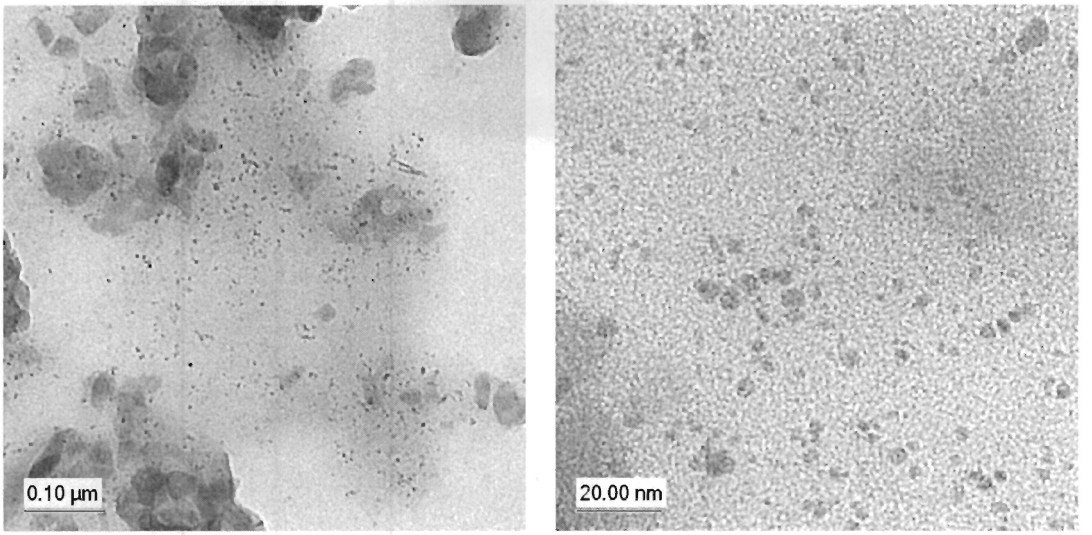

Figure 3-26 Low magnification (left) and higher magnification (right) TEM images of the product prepared with an ultrasound power setting at 20%.

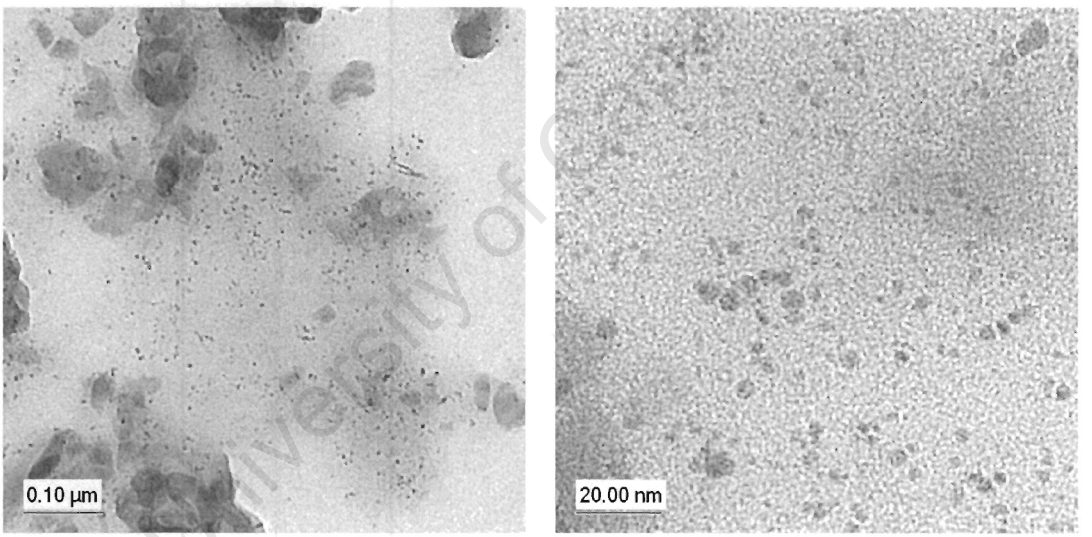

Figure 3-27 Low magnification (left) and higher magnification (right) TEM images of the product prepared with an ultrasound power setting at 60%.

A comparison of the crystallite size distributions of these materials obtained from TEM measurements (Figure 3-28) confirms that there are no significant differences in the crystallite sizes of these materials.

It can perhaps be expected that the ultrasound amplitude may have an effect on the intensity of bubble collapse during ultrasonication. Li-yun et al.[59] observed that they

formed mixed phases at power settings lower than 300 W, but pure hydroxyapatite particles at higher settings. It appears that the ultrasound intensity (amplitude) therefore has a marked influence on their products and that a minimum threshold is necessary to obtain their desired phase. This suggests that the temperature reached during the collapse of the bubbles are influenced by the amplitude setting. One possible explanation why no effect was seen on the synthesis of the cobalt particles can be that the cobalt precursor decomposes at a lower temperature than the precursors used in their study. The lowest amplitude setting used may not have been low enough to decompose only a part of the precursor content within the bubbles.

Table 3-4 Samples prepared at different power settings.

No	Power (%)	Amount of Precursor (g)	Number of measurements	Mean (nm)	Std dev (nm)
A1	20	1.25	1089	1.99	0.72
T1	40	5	651	2.00	0.74
A2	60	1.25	1007	1.84	0.71

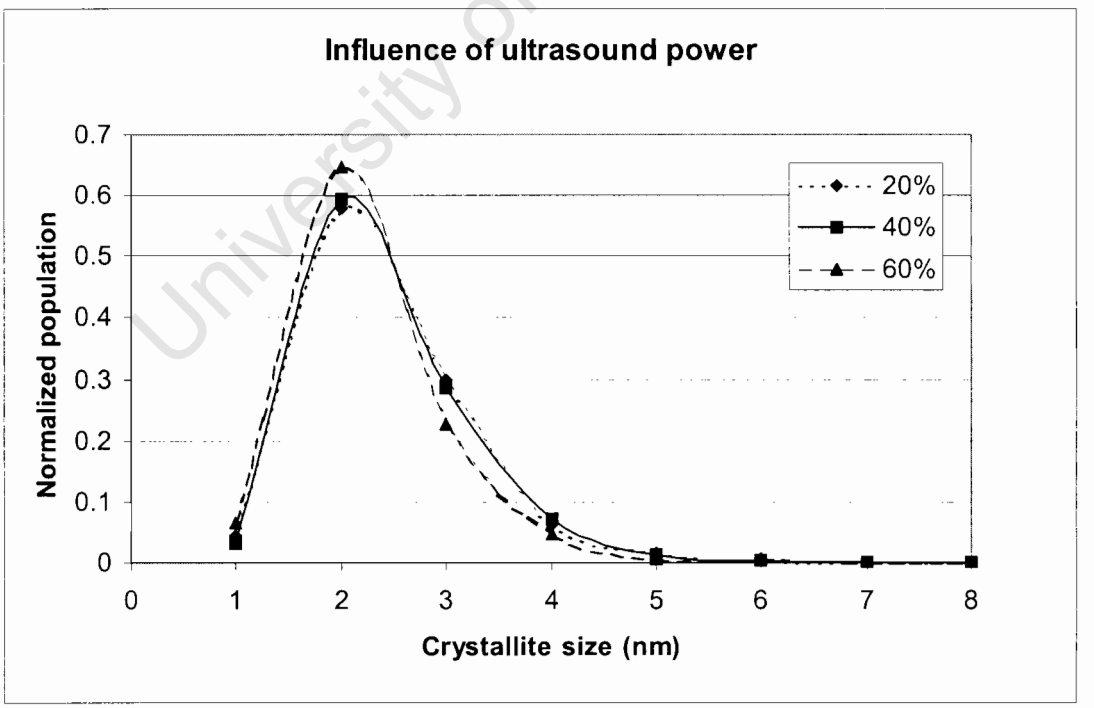

Figure 3-28 Comparison of the crystallite size distributions of materials prepared with different ultrasound power settings.

4 Discussion

In this study the preparation of cobalt crystallites using sonochemical methods was explored. The basis for the preparation of these materials is the evaporation of a metallo-organic compound into a cavity in the liquid. The cavity may grow under ultrasound exposure to form larger bubbles. The collapse of the bubble under adiabatic or close to adiabatic conditions will then lead to decomposition of the metallo-organic compound to the metal.

4.1 Equilibrium radius of bubbles formed by ultrasound

The collapse is induced by resonating the bubble wall movement with the frequency of the sound. The motion of the bubble wall in a sound field is described by the Rayleigh-Plesset equation[37]

$$R\frac{d^2R}{dt^2}+\frac{3}{2}\left(\frac{dR}{dt}\right)^2=\frac{1}{\rho_0}\left[\left(P_0+\frac{2\sigma}{R_0}\right)\left(\frac{R_0}{R}\right)^{3\gamma}-\frac{4\mu}{R}\frac{dR}{dt}-\frac{2\sigma}{R}-\left(P_0-P_A\sin\omega t\right)\right]$$

where R radius of the bubble

t time

ρ_0 density of the liquid

P_0 pressure within the bubble neglecting the Laplace-force, i.e. sum of the vapour pressure of the compounds

σ surface tension at the gas-liquid interface

R_0 radius of the bubble at equilibrium

γ polytropic index of the gas

μ viscosity of the liquid

P_A acoustic pressure

ω acoustic frequency

The resonance bubble frequency is according to Huang et al.[69]:

$$f_r=\frac{1}{2\pi\cdot R_0}\left\{\left[\frac{3\gamma}{\rho_0}\left(P_0+\frac{2\sigma}{R_0}\right)-\frac{2\sigma}{\rho_0\cdot R_0}\right]-\left(\frac{2\mu}{\rho_0\cdot R_0}\right)^2\right\}^{\frac{1}{2}}$$

Thus, the equilibrium radius, R_0, is mainly dependent on the frequency of resonance, i.e. the frequency of ultrasonic radiation (see Figure 4-1), but also on the density, pressure, surface tension and viscosity of the fluid. Under the conditions applied in this study the equilibrium bubble diameter is estimated to be 192.5 μm, assuming that viscosity and surface tension are not strongly dependent on temperature.

Changing γ from 1.67 to 1.4 (e.g. by changing the dissolved gas from argon to nitrogen) will result in a decrease in the equilibrium bubble radius from 192.5 μm to 178.3 μm. Changing the atmospheric pressure from 85 kPa to 100 kPa will result in an increase of the equilibrium bubble diameter from 192.5 μm to 208.8 μm. The surface tension of the liquid and the viscosity of the liquid have only a very small influence on the equilibrium bubble size in this study. The surface tension is not expected to change more than by a few percent[66] and hence have a small influence on the equilibrium bubble size. Furthermore, with the large bubble sizes obtained here, the influence of the surface tension on the bubble size becomes less. The viscosity for n-decane at 10°C is 1.087×10^{-3} Pa·s rather than the viscosity used in the evaluation of the equilibrium radius (at 25 °C 0.838×10^{-3} Pa·s). This does not affect the equilibrium radius of the bubble much since the radius is relatively large.

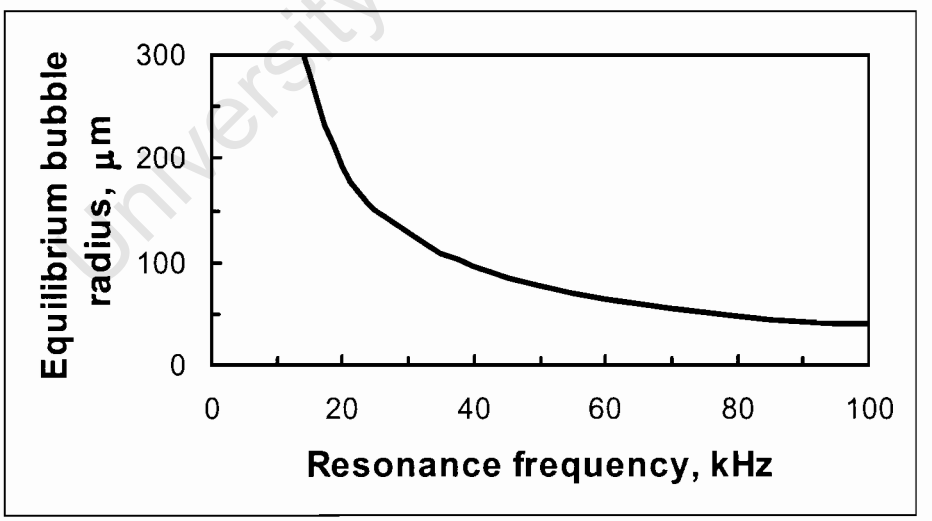

Figure 4-1 Influence of the resonance frequency on the equilibrium bubble size according to Huang et al.[69] ($\gamma = 1.67$, $P_0 = 85$ kPa, $\rho_0 = 730$ kg/m^3, $\sigma = 23.37 \times 10^{-3}$ N/m, $\mu = 0.838 \times 10^{-3}$ Pa·s)

4.2 Evaluation of prepared materials in relation to the equilibrium bubble size

The maximum crystallite diameter is determined by the amount of tricarbonyl nitrosyl cobalt in the bubble before cavitation (assuming the crystallite size is solely determined by this single event). The bubble before cavitation might be considered in the ideal case to be in equilibrium with the liquid, and therefore consist of the dissolved gas (argon), n-decane and the catalyst precursor. The maximum amount of tricarbonyl nitrosyl cobalt is thus given by its equilibrium partial pressure in the bubble.

Suslick et al.[43] prepared iron nano-particles by ultrasonication of a 0.1 M solution of $Fe(CO)_5$ in n-decane. The size of the cavitating bubble is ca. 120 μm in diameter. The vapour pressure of pure $Fe(CO)_5$ at 20 °C is 23.5 Torr. Thus, the vapour pressure of iron carbonyl above a 0.1 M solution of $Fe(CO)_5$ in n-decane is, assuming validity of Raoult's law, 0.45 Torr. Thus, the number of iron atoms in the bubble is given by the ideal gas law:

$$n = \frac{p_{Fe(CO)_5} \cdot V}{R \cdot T} = \frac{\frac{0.45}{760} \cdot 10^5 \cdot \frac{\pi}{6} \cdot \left(120 \cdot 10^{-6}\right)^3}{8.314 \cdot 293.15} = 2.2 \cdot 10^{-14} \cdot mol$$

The size of the resulting iron crystallites can be estimated by assuming spherical geometry:

$$d_{Fe} = \sqrt[3]{\frac{6 \cdot n_{Fe(CO)_5} \cdot M_{Fe}}{\pi \cdot \rho_{Fe}}} = \sqrt[3]{\frac{6 \cdot 2.2 \cdot 10^{-14} \cdot mol \cdot 55.85 \cdot \frac{g}{mol}}{\pi \cdot 7.86 \cdot 10^6 \cdot \frac{g}{m^3}}} = 6.7 \cdot 10^{-7} \cdot m = 67 \cdot nm$$

Crystallites formed by the ultrasonication process are significantly smaller than the value calculated above. Suslick[43] reports crystallites between 3 and 8 nm, which is similar in size to the cobalt crystallites obtained in this study.

Cao et al.[70] prepared iron nanocrystallites by ultrasonication at 20 kHz of pure $Fe(CO)_5$ as well as 4 M, 1 M and 0.25 M mixtures of $Fe(CO)_5$ in decane. This process formed particles consisting of agglomerations of primary particles that were smaller than 25 nm. The size of the agglomerated particles decreased from 243 nm to 59 nm as the concentration of the precursor was decreased.

In this study a number of different methods were applied to synthesize crystallites with a different crystallite size distribution. Table 4-1 shows an overview of the equilibrium bubble size, the expected diameter of the cobalt crystallites and the obtained crystallite sizes. The expected crystallite size based on the equilibrium bubble size is in the μm range, much larger than the nanometer sized crystallites seen in this study. It must thus be concluded that either the bubbles are not in equilibrium with the liquid phase and the amount of metal precursor in these bubbles is much less than predicted according to equilibrium, or that more than one crystallite is formed during cavitation.

Changing the concentration of the precursor in the solution (sample C1 to C4), changes the driving force for its rate of transport to the bubble since this rate is proportional to concentration gradient. The equilibrium radius of the bubble and the average life time of the bubble should remain unchanged upon changing the concentration of $Co(CO)_3(NO)$ in the liquid phase. Therefore, the decrease in the liquid phase concentration is expected to result in a proportional change in the average crystallite size.

Since this change has not been observed in this study, it is deduced that the crystallite size is not determined by the size of the cavitating bubble. Furthermore, the crystallite size of the resulting cobalt metal cannot be related to mass transfer limitations to the bubble followed by the generation of a single crystallite upon the collapse of the bubble. Thus, it is concluded that the collapse of large sized bubbles, as generated in this study, will result in multiple nucleation sites yielding multiple crystallites.

If the bubble is saturated with the metal precursor prior to the collapse, the amount of crystallites formed from a single bubble collapse can be estimated from the maximum expected diameter of the cobalt crystallite and the actual diameter of cobalt crystallites as determined by TEM. This amount is estimated to be between $3x10^7$ and $2x10^{10}$.

Table 4-1 Comparison between the measured average cobalt crystallite size and the maximum crystallite size calculated assuming equilibrium between the equilibrium bubble and the liquid phase.

No.	$x_{Co(CO)_3(NO)}$ [a]	$P_{Co(CO)_3(NO)}$ Pa	T (°C)	r_{Bubble} (μm)	$d_{Co,max}$ [b] (nm)	$d_{Co,average}$ (nm)
t0	0.053	265.1	10	192	3473	5.47
t1	0.007	34.7	10	192	1764	5.5
t2	0.007	34.7	10	192	1764	5.13
t3	0.007	34.7	10	192	1764	5.18
t4	0.007	34.7	10	192	1764	4.55
C1	0.053	265.1	10	192	3473	2.56
C2	0.027	136.1	10	192	2781	2.76
C3	0.014	69.0	10	192	2218	2.85
C4	0.007	34.7	10	192	1764	2.18
T1	0.051	258.4	10	192	3444	2.00
T2	0.014	235.6	35	194	3289	1.86
T3	0.014	688.0	60	197	4639	1.83
A1	0.013	67.2	10	192	2198	1.99
A2	0.013	67.2	10	192	2198	1.84

[a]Mol fraction of cobalt tricarbonyl nitrosyl in the liquid phase

[b]Maximum cobalt crystallite diameter calculated according to:

$$d_{Co,max} = \sqrt[3]{\frac{6 \cdot n_{Co,bubble} \cdot M_{Co}}{\pi \cdot \rho_{Co}}} = \sqrt[3]{\frac{6 \cdot p_{Co(CO)_3(NO)} \cdot \left(\frac{4}{3} \cdot \pi \cdot r_{bubble,equil.}^3\right) M_{Co}}{\pi \cdot \rho_{Co} \cdot R \cdot T}}$$

$$d_{Co,max} = 0.0185 \cdot r_{bubble,equil.} \cdot \sqrt[3]{\frac{p_{Co(CO)_3(NO)}}{T}} \quad \text{(with d in m, p in Pa and T in K)}$$

4.3 Influence of reaction conditions on the cobalt crystallite size

Three different synthesis procedures were used to prepare the cobalt materials and it is interesting to compare the products of these methods with each other. In Figure 4-2 the crystallite size distributions of materials obtained by using the same amount of tricarbonyl nitrosyl cobalt precursor are compared, while Table 4-2 gives a summary of the measurements.

The distributions are clearly different. It is especially surprising that the distribution of the silica-supported material is different from that of the oleic acid-stabilized material since one would expect that both stabilization methods should yield crystallites of the same size. However, Keck et al.[52] have observed that the presence of quartz particles in water has a significant effect on the rate of H_2O_2 formation; at certain frequencies this rate is about 50% higher than the rate for pure water.

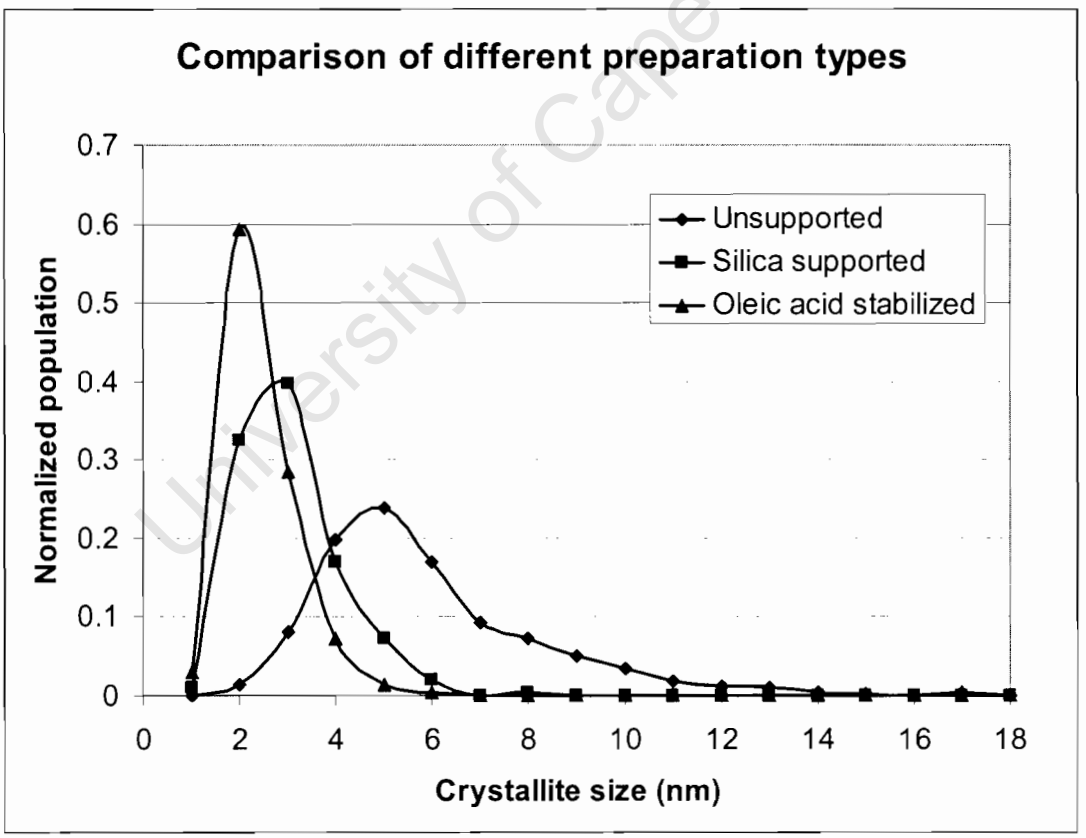

Figure 4-2 Comparison of materials obtained from different preparation methods: Unsupported (sample t0), silica supported (sample C1) and oleic acid stabilized (sample T1).

Table 4-2 Summary of measurements performed on materials prepared using different preparation methods

Sample	Description	Number of measurements	Mean crystallite size (nm)	Std dev (nm)
t0	Unsupported	503	5.47	2.3
T1	Oleic acid stabilized	650	2.00	0.74
C1	Silica supported	206	2.56	1.04

Following the reasoning outlined in the previous section, the collapse of a single bubble yields many small crystallites. In the absence of SiO_2 and oleic acid in the solution, the number of crystallites formed in a single collapse is ca. $4x10^7$.

The introduction of the silica particles results in a 12-fold increase in the number of crystallites formed upon the collapse of a bubble (compare sample C4 with sample t1-t4, see Figure 4-3). It is suspected that the particles introduce new nucleation sites which enhance the formation of cobalt crystallites. At a constant solid content of the liquid (1.5 g/100 ml, samples C2-C4) the estimated number of crystallites formed upon the collapse of the bubble is between 10 and 25 times the number of crystallites formed in absence of the solid. In the preparation of these samples the concentration of the cobalt precursor was changed as well. The increase in the concentration of $Co(CO)_3(NO)$ from 0.625 to 1.25 g/100ml did not result in an increase in the number of crystallites (samples C3-C4). A doubling in the number of crystallites was only observed by increasing the concentration of $Co(CO)_3(NO)$ in the solution from 1.25 to 2.5 g/100ml (C2-C3). Increasing the concentration of $Co(CO)_3(NO)$ even further to 5 g/100 ml and at the same time doubling the solid content to 3 g/100ml resulted again in a doubling of the number of crystallites formed (samples C1-C2).

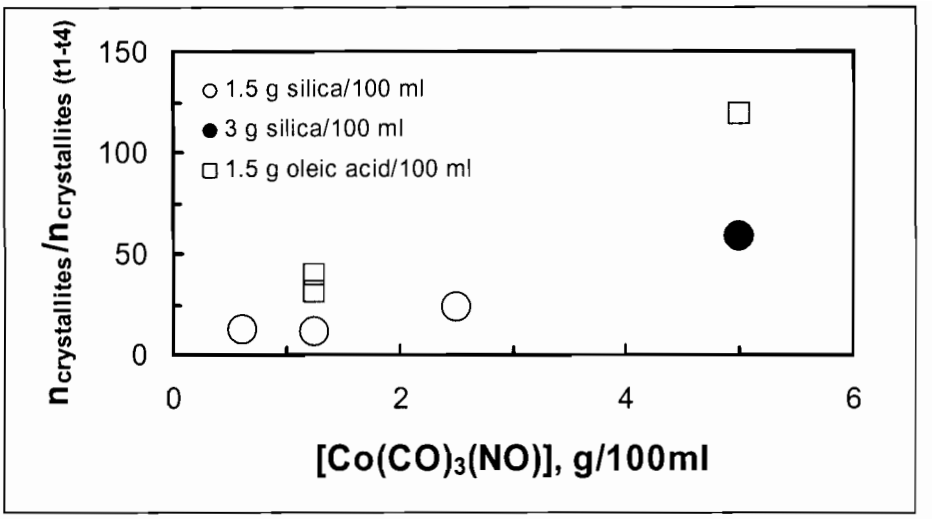

Figure 4-3 Estimated number of crystallites formed upon collapse of a bubble in the presence of SiO_2 or oleic acid relative to the estimated number of crystallites formed in the absence of the solid (average of samples t1-t4) as a function of the liquid phase concentration of $Co(CO)_3(NO)$

The addition of the surfactant, oleic acid, led to a 30- to 40-fold increase in the estimated number of crystallites formed upon the collapse of a bubble (samples A1 and A2). This might be attributed to the stabilisation of the crystallisation nuclei by oleic acid as a surfactant. The presence of oleic acid induces, according to this model, more nuclei than the presence of silica at the same concentration of the cobalt precursor. Hence, oleic acid is more effective at reducing the crystallite size than the addition of silica as a support.

A change in the temperature of the solvent should also affect the viscosity and surface tension of the solvent. However, these changes only marginally affected the equilibrium bubble radius. With increasing temperature only a slight decrease in the average crystallite size, and thus an increase in the estimated number of crystallites upon collapse of the bubble, is observed.

4.4 Controlled synthesis of cobalt crystallites with a narrow crystallite size distribution using sonochemical methods

The results of this study indicate that, at the conditions used, multiple crystallites are formed upon the collapse of the bubble. This results in crystallite sizes equivalent to a crystallization nucleus site. The reaction parameters varied in this system resulted in a change in the number of nuclei rather than in a change in the crystallite size. The number of nuclei can be controlled by the addition of a solid or the addition of oleic acid.

The use of sonochemical methods to obtain controlled crystallite sizes might be obtained with smaller cavitating bubbles, i.e. bubbles of a size less than 0.3 μm. The generation of this size of bubbles would require ultrasound frequencies in excess of 20 MHz. At these ultra-high frequencies it may be possible to control the crystallite size by changing parameters such as the concentration of the metal precursor in the liquid phase, viscosity, surface tension and temperature.

5 Conclusions

In this study, ultrasonication of a tricarbonyl nitrosyl cobalt precursor in n-decane was used to prepare small cobalt crystallites. The aim was to prepare materials with different cobalt crystallite size distributions by varying the ultrasonication conditions. This would then be a useful tool to prepare model cobalt catalysts which can be used to study the oxidation behaviour of small cobalt crystallites during Fischer-Tropsch synthesis reactions.

Straightforward ultrasonication of the cobalt precursor and n-decane solution yielded small amorphous particles (ca. 5 nm) that clump together to form porous structures that are reminiscent of the links in a chain. These nanometer-sized crystallites were much smaller than one would expect from the amount of precursor material that would be present inside the bubble at equilibrium. This raised the possibility that each cavitation event may cause the formation of many crystallites instead of only one.

The influence of ultrasonication time on the crystallite size distribution was investigated using this preparation method. This was done by extracting samples of the product from the reaction vessel at various times ranging from 30 minutes to 20 hours. The samples were kept under inert conditions and simultaneously submitted to a passivation treatment under identical conditions. It was found that the ultrasonication time had no significant influence on the cobalt crystallite size distribution. Since the precursor is gradually depleted during the ultrasonication process, this result was already an indication that the concentration of the precursor in the solvent would not influence the cobalt crystallite size distribution. Furthermore, crystallite growth due to interparticle collisions caused by the ultrasound did not occur.

In an attempt to prevent sintering of the cobalt crystallites, a small amount of silica powder was added to the precursor/solvent solution to act as a support. This resulted in well-dispersed cobalt crystallites stabilized on the silica crystallites, which demonstrated that supported catalyst materials can be effectively prepared using this method. It was found, however, that reduction at 280 °C for four hours during a hydrogen chemisorption analysis resulted in larger cobalt crystallites. Hydrogen chemisorption analysis was thus

not a suitable technique for determining the average cobalt crystallite size. However, this does present an opportunity to tailor the crystallite size distribution of ultrasonically prepared supported materials by a subsequent heat treatment.

The effect of varying the cobalt precursor concentration was investigated by adding different amounts of the precursor (0.625 g to 5 g) to 100 ml of n-decane. The results showed no difference in cobalt crystallite size distribution. As the amount of precursor inside the bubble is dependent on the concentration gradient of the precursor in the solution, this suggested that the crystallite size of the cobalt metal cannot be related to mass transfer limitations or to the precursor content inside the bubble. This supported the hypothesis that more than one crystallite was formed by each cavitation event.

The cobalt crystallites could also be stabilized by adding a small amount of oleic acid to the precursor/solvent mixture prior to ultrasonication. In this way the cobalt crystallites were trapped as colloidal particles right after they were formed.

It was interesting to note that the size distributions of the cobalt crystallites formed by the unsupported, silica-supported and oleic acid-stabilized processes were significantly different. It was suggested that the presence of silica particles or the oleic acid surfactant caused more nucleation sites and consequently more, but smaller, crystallites.

The temperature of the precursor/n-decane solution was varied between 10 °C and 60 °C. This had no effect on the crystallite size distribution. Since an increase in temperature would have changed the amount of cobalt precursor vapour inside the collapsing bubble, this again confirmed that the crystallite size distribution is independent of the precursor concentration inside the bubble. Furthermore, an increase in temperature also changes the viscosity of the solution, which implies that this property also has no effect on the cobalt crystallites formed.

The ultrasound amplitude was varied between 20% and 60% of maximum that can be delivered by the equipment. Again no effect was seen on the cobalt crystallite size distribution.

6 References

[1] Dry ME, *Catalysis Today* **71** (2002), 227-241

[2] Colitti M, *Natural Gas Conversion IV: Studies in Surface Science and Catalysis* **107** (1997), 1-4

[3] Schulz H, *Applied Catalysis A: General* **186** (1999), 3-12

[4] Anderson RB, *The Fischer-Tropsch Synthesis*, Academic Press, Inc., Orlando, Florida, 1984

[5] Dry ME, in: Anderson JR, Boudart M (Eds.), *Catalysis Science and Technology*, Springer Verlag, New York, 1981, 159

[6] Dry ME, *Applied Catalysis A: General* **138** (1996), 319-344

[7] Dry ME, *Applied Catalysis A: General* **189** (1999), 185-190

[8] Gradassi MJ, *Natural Gas Conversion IV: Studies in Surface Science and Catalysis* **119** (1998), 35-44

[9] Jager B, *Natural Gas Conversion IV: Studies in Surface Science and Catalysis* **119** (1998), 25-34

[10] Espinoza RL, Steynberg AP, Jager B and Vosloo AC, *Applied Catalysis A: General* **186** (1999), 13-26

[11] Jager B and Espinoza R, *Catalysis Today* **23** (1995), 17-28

[12] Vannice MA, *Journal of Catalysis* **37** (1975), 449-461

[13] Adesina AA, *Applied Catalysis A: Gene*ral **138** (1996), 345-367

[14] Van Berge PJ and Everson RC, *Natural Gas Conversion IV: Studies in Surface Science and Catalysis* **107** (1997), 207-212

[15] Yates I and Satterfield CN, *Energy and Fuels* **5** (1991), 168

[16] Iglesia E, *Applied Catalysis A: General* **161** (1997), 59-78

[17] Van Berge PJ, van de Loosdrecht J, Barradas S and van der Kraan AM, *Catalysis Today* **58** (2000), 321-334

[18] Van Steen E, Claeys M, Dry M, van de Loosdrecht J, Viljoen E and Visagie J, *Journal of Physical Chemistry B* **109** (2005), 3575-3577

[19] Arnoldy P and Moulijn JA, *Journal of Catalysis* **93** (1985), 38-54

[20] Schanke D, Hilmen AM, Bergene E, Kinnari K, Rytter E, Adnanes E and Holmen A, *Catalysis Letters* **34** (1995), 269-284

[21] Tung HC, Yeh CT and Hong CT, *Journal of Catalysis* **122** (1990), 211-216

[22] Hilmen AM, Schanke D, Hanssen KF and Holmen A, *Applied Catalysis A: General* **186** (1999), 169-188

[23] Jongsomjit B, Panpranot J and Goodwin JG Jr., *Journal of Catalysis* **204** (2001), 98-109

[24] Jacobs G, Patterson PM, Zhang Y, Das T, Li J and Davis BH, *Applied Catalysis A: General* **233** (2002), 215-226

[25] Li J, Zhan X, Zhang Y, Jacobs G, Das T and Davis BH, *Applied Catalysis A: General* **228** (2002), 203-212

[26] Hilmen AM, Schanke D and Holmen A, *Natural Gas Conversion IV: Studies in Surface Science and Catalysis* **107** (1997), 237-242

[27] Zhang Y, Wei D, Hammache S and Goodwin JG Jr., *Journal of Catalysis* **188** (1999), 281-290

[28] Schanke D, Vada S, Blekkan EA, Hilmen AM, Hoff A and Holmen A, *Journal of Catalysis* **156** (1995), 85-95

[29] Richards WT and Loomis AL, *Journal of the American Chemical Society* **49** (1927), 3086-3100

[30] Frenzel H and Schultes H, *Zeitschrift für Physikalische Chemie B* **27** (1935), 421-424

[31] Sehgal C, Sutherland RG and Verrall RE, *Journal of Physical Chemistry* **84** (1980), 388-395

[32] Henglein A, *Ultrasonics* **25** (1987), 6-16

[33] Suslick KS and Kemper KA, *Ultrasonics* **31** (1993), 463-465

[34] Suslick KS, *MRS Bulletin* **20** (1995), 29-34

[35] Suslick KS, Doktycz SJ and Flint EB, *Ultrasonics* **28** (1990), 280-290

[36] Suslick KS, *Scientific American*, February 1989, 62-68

[37] Neppiras EA, *Physics Reports* **61** (1980), 159-251

[38] Suslick KS, Hammerton DA and Cline RE Jr., *Journal of the American Chemical Society* **108** (1986), 5641-5642

[39] Barber BP and Putterman SJ, *Nature* **352** (1991), 318-320

[40] Suslick KS, *Science* **247** (1990), 1439-1445

[41] Lauterborn W and Vogel A, *Annual Review of Fluid Mechanics* **16** (1984), 223-244

[42] Doktycz SJ and Suslick KS, *Science* **247** (1990), 1067-1069

[43] Suslick KS, Hyeon T, Fang M and Cichowlas AA, *Advanced Catalysts and Nanostructures Materials : Modern synthetic methods*, 1996 Academic Press Inc.

[44] Shafi KVPM, Gedanken A, Prozorov R, Revesz A and Lendvai J, *Journal of Materials Research* **15** (1999), 332-337

[45] Wang H, Zang J, Zhao X, Xu S and Zhu J, *Materials Letters* **55** (2002), 253-258

[46] Wang H, Zang J and Zhu J, *Journal of Crystal Growth* **246** (2002), 161-168

[47] Gutierrez M and Henglein A, *Ultrasonics* **27** (1989), 259-261

[48] Lindley J, *Ultrasonics* **30** (1992), 163-167

[49] Amara N, Ratsimba B, Wilhelm A and Delmas H, *Ultrasonics Sonochemistry* **8** (2001), 265-270

[50] Bianchi CL, Martini F and Ragaini V, *Ultrasonics Sonochemistry* **8** (2001), 131-135

[51] Petrier C and Francony A, *Ultrasonics Sonochemistry* **4** (1997), 295-300

[52] Keck A, Gilbert E and Koster R, *Ultrasonics* **40** (2002), 661-665

[53] Hofmann J, Freier U and Wecks M, *Ultrasonics Sonochemistry* **10** (2003), 271-275

[54] Shafi KVPM, Gedanken A, Prozorov R, *Journal of Materials Chemistry* **8** (1998), 769-773

[55] Gedanken A, *Current Science* **85** (2003), 1720-1722

[56] Takatani H, Kago H, Nakanishi M, Kobayashi Y, Hori F and Oshima R, *Reviews on Advanced Materials Science* **5** (2003), 232 - 238

[57] Grinstaff MW, Cichowlas AA, Choe SB and Suslick KS, *Ultrasonics* **30** (1992), 168-172

[58] Didenko YT, Nastich DN, Pugach SP, Polovinka YA and Kvochka VI, *Ultrasonics* **32** (1994), 71-76

[59] Li-yun C, Chuan-bo Z and Jian-feng H, *Materials letters* **59** (2005), 1902-1906

[60] Li B, Xie Y, Huang J, Liu Y, Qian Y, *Ultrasonics Sonochemistry* **8** (2001), 331-334

[61] Zhang J, Liu Z, Han B, Jiang T, Wu W, Chen J Li Z and Liu D, *Journal of Physical Chemistry B* **108** (2004), 2200-2204

[62] Wang H, Zhu J, Zhu J, Liao X, Xu S, Ding T and Chen H, *Physical Chemistry Chemical Physics* **4** (2002), 3794 - 3799

[63] Van Berge PJ, van de Loosdrecht J, Visagie JL, WO 01/96014, 2001

[64] High Intensity Ultrasonics Processer User's guide, Sonics and Materials Inc.

[65] Ivanova AR, Nuesca G, Chen X, Goldberg C, Kaloyeros AE, Arkles B and Sullivan JJ, *Journal of the Electrochemical Society* **146** (1999), 2139-2145

[66] Liley, PE, Thomson, GH, Friend, DG, Daubert, TE, and Buck, E, in "*Perry's Chemical Engineers' Handbook*" (Editors: R.H. Perry, D.W. Green, J.O. Maloney), 7th ed., Mc-Graw-Hill, New York, 1997

[67] Van Steen E, Sewell GS, Makhothe RA, Micklethwaite C, Manstein H, de Lange M and O'Connor CT, *Journal of Catalysis* **162** (1996), 220-229

[68] Koltypin Y, Nikitenko SI and Gedanken A, *Journal of Materials Chemistry* **12** (2002), 1107-1110

[69] Huang J, Feng R, Zhu C and Chen Z, *Ultrasonics Sonochemistry* **2** (1995), 93-97

[70] Cao X, Koltypin Y, Kataby G, Prozorov R, Gedanken A, *Journal of Materials Research* **10** (1995), 2952-2957

[71] Anderson JR, *Structure of Metallic Catalysts*, Academic Press Inc., London, 1975

Appendix

Calculation of crystallite size from chemisorption measurements

The following are needed for the calculation :

Density (ρ) of cobalt metal = 8.9 g/cm^3

Avogadro's number = 6.023x10^{23}

Concentration of surface atoms[71] = 1.51x10^{19} atoms/m^2 = 2.507x10^{-9} mol/cm^2

Mass of cobalt per gram sample (determined using ICP analysis) = 0.067 g

The volume of cobalt per gram of catalyst is calculated by :

$$V = \frac{m}{\rho} = \frac{0.067}{8.9} = 7.52 \times 10^{-3} cm^3$$

The volume of H_2 adsorbed per gram of catalyst during the chemisorption analysis was determined by linearising the Langmuir equation (given in section 3.2.2):

$$\frac{1}{V} = \frac{1}{V_m K P_{H2}^{\frac{1}{2}}} + \frac{1}{V_m}$$

The data from the hydrogen chemisorption profile were converted into this form by plotting a graph of 1/V vs $1/P^{0.5}$ and the value of V_m, the volume of hydrogen adsorbed, was determined from the intercept with the y-axis as 1.530 cm^3.

1 mol of gas at STP has a volume of 22400 cm^3. Thus, the number of hydrogen molecules adsorbed is 1.530/22400 = 6.83x10^{-5} mol. Since hydrogen adsorbs dissociatively, this means that 6.83x10^{-5}x2 = 1.366x10^{-4} hydrogen atoms were adsorbed.

The area of the adsorbed atoms, assuming that one hydrogen atoms adsorps onto one cobalt surface atom, is determined by :

$$A = \frac{n_{ads} \times stoichiometry}{conc} = \frac{1.366 \times 10^{-4} \times 1}{2.507 \times 10^{-9}} = 54490 cm^2$$

Assuming the particles are spherical, the diameter of a sphere with the same volume-to-surface ratio as the cobalt in the material is given by :

$$d_{VA} = \frac{6V}{A} = \frac{6 \times 7.52 \times 10^{-3}}{47651} = 8.28 \times 10^{-7} cm = 8.3nm$$